
Message-Passing State-Space Models: Improving Graph Learning with Modern Sequence Modeling

Andrea Ceni
 University of Pisa
 andrea.ceni@unipi.it

Alessio Gravina
 University of Pisa
 alessio.gravina@di.unipi.it

Claudio Gallicchio
 University of Pisa
 claudio.gallicchio@unipi.it

Davide Bacciu
 University of Pisa
 davide.bacciu@unipi.it

Carola-Bibiane Schönlieb
 University of Cambridge
 cbs31@cam.ac.uk

Moshe Eliasof
 University of Cambridge
 me532@cam.ac.uk

Abstract

The recent success of State-Space Models (SSMs) in sequence modeling has motivated their adaptation to graph learning, giving rise to Graph State-Space Models (GSSMs). However, existing GSSMs operate by applying SSM modules to sequences extracted from graphs, often compromising core properties such as permutation equivariance, message-passing compatibility, and computational efficiency. In this paper, we introduce a new perspective by embedding the key principles of modern SSM computation directly into the Message-Passing Neural Network framework, resulting in a unified methodology for both static and temporal graphs. Our approach, MP-SSM, enables efficient, permutation-equivariant, and long-range information propagation while preserving the architectural simplicity of message passing. Crucially, MP-SSM enables an exact sensitivity analysis, which we use to theoretically characterize information flow and evaluate issues like vanishing gradients and over-squashing in the deep regime. Furthermore, our design choices allow for a highly optimized parallel implementation akin to modern SSMs. We validate MP-SSM across a wide range of tasks, including node classification, graph property prediction, long-range benchmarks, and spatiotemporal forecasting, demonstrating both its versatility and strong empirical performance.

1 Introduction

Graph Neural Networks (GNNs), especially Message-Passing Neural Networks (MPNNs), have become a staple in learning from graph-structured data. However, traditional MPNNs like GCNs [61] face challenges in propagating information across distant nodes due to issues such as over-squashing [2, 105, 27] and vanishing gradients [27, 84, 3], which hinder performance in tasks requiring long-range dependency modeling [32]. While various strategies—such as rewiring [105, 60, 49], transformers [64, 118, 88, 33, 31], and weight-space regularization [43, 44] have been proposed to improve signal propagation, a principled and simple solution to overcome these issues of MPNNs remains elusive, in the sense that most aforementioned methods require significant architectural modifications, and cannot be applied to traditional MPNNs like GCN [61].

In parallel, recent breakthroughs in sequence modeling using State-Space Models (SSMs)—e.g., LRU [81], S4 [46], and extensions [97, 48, 87, 38]—have led to advanced architectures like Mamba [45], Griffin [25], and xLSTM [9]. These models consist of stacked recurrent seq2seq blocks, moving nonlinearities outside the recurrence [4] and interleaving them with multilayer perceptrons (MLPs), enabling long-range dependency modeling, stable gradient flow, efficient training, and universal approximation [80, 77]. This design balances short-term memory retention [59] and nonlinear expressivity [58, 24]—a trade-off critical to learn long-term dependencies while representing complex nonlinear relationships within data [85, 109].

Inspired by these advances, researchers have begun tailoring SSMs for graph learning. Some approaches adopt spectral methods [57], while others transform graphs into sequences for SSM processing [103, 110, 10], often compromising permutation-equivariance [14] or graph topology. Alternatives like GrassNet [121] rely on spectral decompositions with non-unique modes [69], limiting generality. In this paper, we propose a novel approach that enhances the traditional MPNN paradigm by integrating modern SSM heuristics, resulting in a general and principled framework for their unification.

The contributions of this paper are:

1. **Unifying Static and Temporal Graphs via a Principled Integration of SSMs and MPNNs.** We propose the Message-Passing State-Space Model (MP-SSM), a principled framework that integrates SSMs into MPNNs. MP-SSM is grounded in a linear diffusion process over the graph, followed by a nonlinear, graph-agnostic transformation. This design preserves permutation equivariance and graph topology, enabling stable long-range information propagation, overcoming key limitations of prior graph SSMs, and supporting a fast parallel implementation akin to standard SSMs.
2. **Exact Sensitivity Analysis.** MP-SSM admits exact Jacobian computations for node-to-node dependencies, allowing for precise estimations of vanishing gradient effects and over-squashing in the deep regime—issues that commonly hinder expressive power in deep GNNs. Unlike most results in the literature, which offer loose upper bounds with limited insight into information transfer across the graph, we provide lower bounds on the spectral norm of the Jacobian—offering a more precise and informative characterization.
3. **Strong Empirical Results.** We validate MP-SSM across 15 synthetic and real-world benchmarks. MP-SSM achieves state-of-the-art performance on long-range synthetic benchmarks, LRGB, heterophilic datasets, and multivariate time series forecasting—demonstrating its versatility and robustness.

2 Message-Passing State-Space Model

We introduce a framework that brings modern SSM principles to graphs, while generalizing the traditional MPNN paradigm. We call our approach *Message-Passing State-Space Model* (MP-SSM).

Graph and Shift Operator. We represent a graph as $G = (V, E)$ where V is a set of n nodes, and $E \subseteq V \times V$ is a set of m undirected edges. The adjacency matrix $\tilde{\mathbf{A}} \in \{0, 1\}^{n \times n}$ encodes edge presence with $(\tilde{\mathbf{A}})_{ij} = 1$ if $(i, j) \in E$, and zero otherwise. To enable message passing, we use the graph shift operator (GSO) defined as the symmetrically normalized adjacency with self-loops [61]:

$$\mathbf{A} = \mathbf{D}^{-\frac{1}{2}}(\tilde{\mathbf{A}} + \mathbf{I})\mathbf{D}^{-\frac{1}{2}}, \quad (1)$$

where $\tilde{\mathbf{A}}$ is the adjacency matrix, and \mathbf{D} is the degree matrix of $\tilde{\mathbf{A}} + \mathbf{I}$, with $(\mathbf{D}^{-\frac{1}{2}})_{ii} = (1 + \sum_{j=1}^n (\tilde{\mathbf{A}})_{ij})^{-\frac{1}{2}}$. The framework we propose applies to any GSO. Our choice of the symmetrically normalized adjacency with self-loops as GSO is due to its popularity and simplicity.

Linear State-Space Recurrence on Graphs We denote the graph data as a sequence of input node features $[\mathbf{U}_t]_{t=1}^T$, with $\mathbf{U}_t \in \mathbb{R}^{n \times c'}$, with c' being the dimensionality of the input features. We note that, for static graphs the sequence consists of a single element, i.e., \mathbf{U}_1 . We embed the sequence of input states, obtaining a sequence of hidden states $[\mathbf{X}_t]_{t=1}^T$, where $\mathbf{X}_t \in \mathbb{R}^{n \times c}$, via a linear

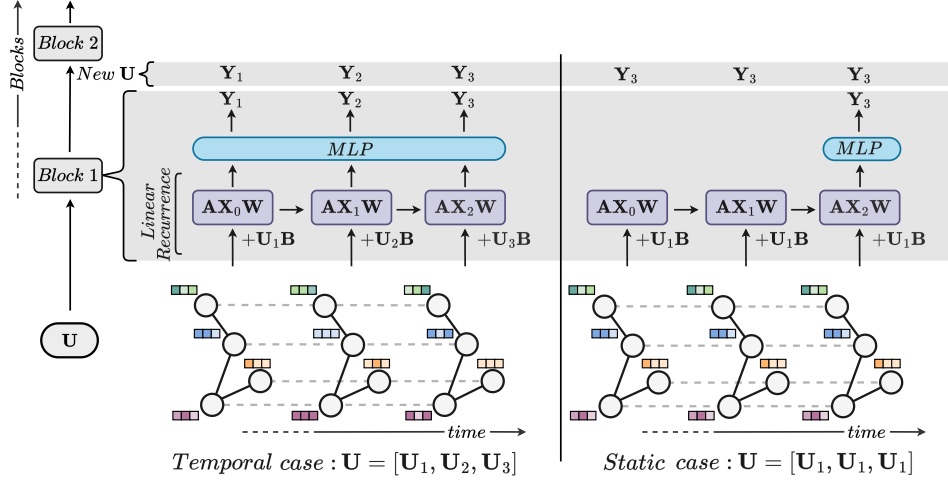


Figure 1: Illustration of our MP-SSM for temporal and static cases, considering a recurrence time $k + 1 = 3$. The temporal case (left) incorporates dynamic updates to node embeddings over time steps, represented as $\mathbf{U} = [\mathbf{U}_1, \mathbf{U}_2, \mathbf{U}_3]$, while the static case (right) uses fixed node embeddings $\mathbf{U} = [\mathbf{U}_1, \mathbf{U}_1, \mathbf{U}_1]$. An MP-SSM block comprises a linear recurrence followed by a multilayer perceptron (MLP). Multiple MP-SSM blocks are stacked to construct a deep MP-SSM architecture.

message-passing scheme and channel mixing with learnable weight matrices $\mathbf{W} \in \mathbb{R}^{c \times c}$, $\mathbf{B} \in \mathbb{R}^{c' \times c}$, as follows:

$$\mathbf{X}_{t+1} = \mathbf{A}\mathbf{X}_t\mathbf{W} + \mathbf{U}_{t+1}\mathbf{B}. \quad (2)$$

Equation (2) represents the linear state-space recurrence on graphs. Note that the message-passing mechanism of many popular GNN models in the literature can be expressed through the form of this equation, including methods like GCN [61], GAT [108], and GIN [117]. A key distinction from such models lies in the use of a purely linear recurrent equation. This design choice is consistent with modern SSM approaches and, crucially, enables both an exact sensitivity analysis (discussed in Section 3) and an efficient parallel implementation. Specifically, MP-SSM can be parallelised by unrolling the linear recurrence and computing a closed-form solution in a single step. In Appendix B, we describe our fast implementation, discussing both its advantages and limitations, and provide a runtime comparison with a standard GCN, showing that MP-SSM can achieve up to a 1000 \times speedup.

MP-SSM Block. A block of our MP-SSM is designed to propagate information between nodes that are k hops away from each other, where k can also be large, as discussed in Section 3. Each block is composed of k iterations of the linear recurrence described in Equation (2), followed by a learnable graph-agnostic nonlinear mapping. Setting the initial state $\mathbf{X}_0 = \mathbf{0} \in \mathbb{R}^{n \times c}$, we define our MP-SSM block as:

$$\mathbf{X}_{t+1} = \mathbf{A}\mathbf{X}_t\mathbf{W} + \mathbf{U}_{t+1}\mathbf{B}, \quad t = 0, \dots, k, \quad (3)$$

$$\mathbf{Y}_{t+1} = \text{MLP}(\mathbf{X}_{t+1}), \quad (4)$$

where MLP denotes a nonlinear multilayer perceptron of 2 dense layers with a nonlinearity in between them, and k a hyperparameter defining the depth of each MP-SSM block. Equations (3) and (4) define the state-space representation on graphs, which forms the foundation of our proposed MP-SSM. Our framework is inspired by SSMs, which are naturally suited for sequential data. In temporal graph settings, the input naturally consists of a sequence of graphs (e.g., with time-varying features). Given an input sequence $\mathbf{U} = [\mathbf{U}_1, \mathbf{U}_2, \dots, \mathbf{U}_{k+1}]$, we apply the same MLP decoder of Equation (4), shared across all time steps, to the corresponding embeddings $[\mathbf{X}_1, \mathbf{X}_2, \dots, \mathbf{X}_{k+1}]$, producing an output sequence $[\mathbf{Y}_1, \mathbf{Y}_2, \dots, \mathbf{Y}_{k+1}]$ of the same length. For static graphs, however, we must construct a sequence from a single input instance \mathbf{U}_1 . As illustrated in Figure 1, we unify the treatment of temporal and static settings by generating a constant input sequence $\mathbf{U} = [\mathbf{U}_1, \mathbf{U}_1, \dots, \mathbf{U}_1]$ of length $k + 1$ for the static case. This design induces a skip connection in the recurrence, which plays a crucial role in mitigating oversmoothing when using the GSO defined in Equation (1). In the static setting, the MLP decoder is applied solely to the final embedding after $k + 1$ steps. Consequently, both the

input and output sequences are constant: $[\mathbf{U}_1, \mathbf{U}_1, \dots, \mathbf{U}_1]$ as input and $[\mathbf{Y}_{k+1}, \mathbf{Y}_{k+1}, \dots, \mathbf{Y}_{k+1}]$ as output. Figure 1 illustrates and summarizes the modes of operation described above. In Appendix C we clarify the originality of our method in relation to recent temporal graph that use a state-space modeling approach, like GGRNN [90] and GraphSSM [66]. One key feature that distinguishes MP-SSM from all other approaches is the absence of nonlinearity in the graph diffusion dynamics. In fact, the only nonlinearity in the entire MP-SSM block resides within the MLP decoder. This is also essential for enabling efficient parallel implementation of the recurrence, as detailed in Appendix B.

The Deep MP-SSM Architecture. Following principles established in modern SSMs [46, 81], we build a hierarchy of representations by constructing a deep MP-SSM architecture composed of stacked MP-SSM blocks. We use the output of an MP-SSM block as an input for the next one. We visually summarize this concept at the top of Figure 1. We note that, stacking multiple MP-SSM blocks allows the model to increase its effective aperture, aggregating information from further nodes. Specifically, the embedding \mathbf{Y}_{k+1} encodes information aggregated up to the k -th hop. Therefore, stacking s MP-SSM blocks, each of depth k , allows to aggregate information from up to sk hops away. In Appendix D, we provide a multi-hop interpretation of a deep MP-SSM architecture, in the static case.

MP-SSM generalizes MPNNs. We note that our MP-SSM can implement its backbone MPNN, an important property that allows it to retain desired or known behavior from existing MPNNs while also generalizing it and allowing for improved information transfer, as discussed in Section 3. To show that our model can implement its backbone MPNN, which in our case is based on GCN via the chosen GSO (as shown in Equation (1)), we consider the static case, i.e., an input sequence $[\mathbf{U}_1, \dots, \mathbf{U}_1]$, under the assumption that the MLP is a nonlinear activation σ function. We note that this can be obtained if the weights within the MLP decoder are the identity matrices, i.e., $\text{MLP}(\cdot) = \sigma(\cdot)$. Then an MP-SSM block with $k = 1$ yields a GCN layer. In fact, if $k = 1$ then Equations (3) and (4) read:

$$\mathbf{X}_1 = \mathbf{U}_1 \mathbf{B} \quad \Rightarrow \quad \mathbf{X}_2 = \mathbf{A} \mathbf{U}_1 \mathbf{B} \mathbf{W} + \mathbf{U}_1 \mathbf{B} = \mathbf{A} \mathbf{X}_1 \mathbf{W} + \mathbf{X}_1 \quad \Rightarrow \quad \mathbf{Y}_2 = \sigma(\mathbf{A} \mathbf{X}_1 \mathbf{W} + \mathbf{X}_1),$$

which implements a GCN with a residual connection. Then \mathbf{Y}_2 is passed as an input to the next MP-SSM block, which yields a similar update rule, effectively constructing a deep GCN. However, we note that if $k \geq 2$, then an MP-SSM block deviates from the standard GCN processing.

Final SSM heuristics. If the GSO is the identity matrix ($\mathbf{A} = \mathbf{I}$), then stacking s MP-SSM blocks with one recurrence each ($k = 1$) results in a deep MLP of depth $2s$. This feedforward architecture is graph-agnostic, and it can be made resilient to vanishing and exploding gradient issues through standard deep learning heuristics such as residual connections [52] and normalization layers [107], with dropout being employed as a regularization technique to support the learning of robust hierarchical representations [100]. In our deep MP-SSM architecture, we apply these heuristics between MP-SSM blocks, following established practices in SSMs [46, 45]. Appendix E presents an ablation study tracing the incremental impact of each SSM heuristic on graph representation learning, progressing from a plain GCN to a deep MP-SSM architecture. Finally, we discuss the complexity and runtimes of MP-SSM in Appendix F.

3 Sensitivity Analysis

We conduct a sensitivity analysis of MP-SSM via the spectral norm of the Jacobian of node features, as in [105]. We provide an exact characterization of MP-SSM’s gradient flow through the graph, identify unfavourable topological structures that intensify oversquashing effects, and quantitatively assess the impact of removing nonlinearities at each recurrent step of graph diffusion, particularly in alleviating vanishing gradients in the deep regime.

Remark 3.1. As discussed in Section 2, MP-SSM extends graph-agnostic deep feedforward networks, for which established deep learning heuristics are known to effectively address vanishing/exploding gradient issues. This observation motivates our focus for sensitivity analysis on the linear recurrent equation within an MP-SSM block, as it encapsulates the core dynamics relevant to information propagation on graphs. Notably, all the other operations within a deep MP-SSM are independent of the graph structure. Thus, **if the linear recurrent equation supports effective information transfer, then this property naturally extends across the full MP-SSM architecture**, which is fundamentally a stack of such linear recurrences.

Let $\mathbf{X}_s^{(j)}$ and $\mathbf{X}_t^{(i)}$ denote the embeddings of nodes j and i at time steps $s \leq t$. We define:

Definition 3.2 (Local sensitivity). The *local sensitivity* of the features of the i -th node to features of the j -th node, after $t - s$ applications of message-passing aggregations, is defined as the following spectral norm:

$$\mathcal{S}_{ij}(t - s) = \left\| \frac{\partial \mathbf{X}_t^{(i)}}{\partial \mathbf{X}_s^{(j)}} \right\|. \quad (5)$$

Equation (5) measures the influence of node j 's features at time s on node i at time t .

Remark 3.3. If the local sensitivity between two nodes increases exponentially with $t - s$, then the learning dynamics of the MPNN are unstable; that is the typical case for linear MPNNs using the adjacency matrix without any normalization or feature normalization. Therefore, **upper bounds on local sensitivity are linked with stable message propagation, in the deep regime.**

The linearity of the recurrence of an MP-SSM block allows an exact computation of the Jacobian between two nodes j, i at different times s, t , in terms of the powers of the GSO, as expressed by Equation (6) in Theorem 3.4 (for the proof, see Appendix A.2).

Theorem 3.4 (Exact Jacobian computation in MP-SSM). *The Jacobian of the linear recurrent equation of an MP-SSM block, from node j at layer s to node i at layer $t \geq s$, can be computed exactly, and it has the following form:*

$$\frac{\partial \mathbf{X}_t^{(i)}}{\partial \mathbf{X}_s^{(j)}} = \underbrace{(\mathbf{A}^{t-s})_{ij}}_{\text{scalar}} \underbrace{(\mathbf{W}^\top)^{t-s}}_{\text{matrix}}. \quad (6)$$

Consequently, GSOs that yield a bounded outcome under iterative multiplication promote stable MP-SSM dynamics, as highlighted in Remark 3.3. In Lemma 3.5, we formally prove (see Appendix A.1) that the GSO defined in Equation (1) exhibits this stability property, along with additional characteristics¹ that support our theoretical analysis.

Lemma 3.5 (Powers of symmetrically normalized adjacency with self-loops). *Assume an undirected graph. The spectrum of the powers of the symmetric normalized adjacency matrix $\mathbf{A} = \mathbf{D}^{-\frac{1}{2}}(\tilde{\mathbf{A}} + \mathbf{I})\mathbf{D}^{-\frac{1}{2}}$ is contained in the interval $[-1, 1]$. The largest eigenvalue of \mathbf{A}^t has absolute value of 1 with corresponding eigenvector $\mathbf{d} = \text{diag}(\mathbf{D}^{\frac{1}{2}})$, for all $t \geq 1$. In particular, the sequence of powers $[\mathbf{A}^t]_{t \geq 1}$ does not diverge or converge to the null matrix.*

Thus, Lemma 3.5 implies that the symmetrically normalized adjacency with self-loops, i.e., Equation (1), serves as a GSO that ensures stable dynamics when performing a large number of message-passing operations in the MP-SSM's framework. Moreover, for such a particular GSO, we can derive a precise approximation of the local sensitivity in the deep regime, as stated in Theorem 3.6 and proved in Appendix A.3.

Theorem 3.6 (Approximation deep regime). *Assume a connected graph, and the GSO defined in Equation (1). Then, for large values of $t - s$, the Jacobian of the linear recurrent equation of an MP-SSM block, from node j at layer s to node i at layer $t \geq s$, admits the following approximation:*

$$\frac{\partial \mathbf{X}_t^{(i)}}{\partial \mathbf{X}_s^{(j)}} \approx \frac{\sqrt{(1 + d_i)(1 + d_j)}}{|V| + 2|E|} (\mathbf{W}^\top)^{t-s}, \quad (7)$$

where $d_l = \sum_{j=1}^n (\tilde{\mathbf{A}})_{lj}$ is the degree of the l -th node.

For the case of the GSO of Equation (1), we can find a precise lower bound for the minimum local sensitivity among all possible pairs of nodes in the graph, in the deep regime (proof in Appendix A.4).

Corollary 3.7 (Lower bound minimum sensitivity). *Assume a connected graph, and the GSO of Equation (1). Then, for large values of $t - s$, the following lower bound for the minimum local sensitivity of the linear recurrent equation of an MP-SSM block holds:*

$$\frac{2}{|V| + 2|E|} \|\mathbf{W}^{t-s}\| \leq \min_{i,j} \mathcal{S}_{ij}(t - s). \quad (8)$$

¹Similar characteristics of the GSO in Equation (1) have also been discussed in [79].

The minimum local sensitivity is realized for pairs of nodes among which the transfer of information is the most critical due to the structure of the graph. Therefore, **lower bounds on the minimum local sensitivity are linked to the alleviation of over-squashing**. Rewiring techniques are known to help combating this phenomenon [27]. Corollary 3.7 proves that, without rewiring, MP-SSM can deal with over-squashing by increasing the norm of the recurrent weight matrix. In Remark 3.8, we construct an example of a topology that approaches the lower bound of Equation (8), thus realising a worst case scenario due to over-squashing.

Remark 3.8 (Bottleneck Topologies). A chain of m cliques of order d represents a topology realising a bad scenario for Equation (7), since local sensitivity can reach values as low as $\frac{1}{md^2}$, scaling on long chains and large cliques, see Appendix A.3.1 for details. This effect is intrinsically tied to the specific topology of the graph, and it aligns with prior studies that emphasize the challenges of learning on graphs with bottleneck structures [105].

To assess the overall gradient information flow across the entire graph in the deep regime, we define:

Definition 3.9 (Global sensitivity). The *global sensitivity* of node features of the overall graph after $t - s$ hops of message aggregation is defined as:

$$\mathcal{S}(t - s) = \max_{i,j} \mathcal{S}_{ij}(t - s). \quad (9)$$

Remark 3.10. The local sensitivity between two far-apart nodes can be physiologically small due to the particular topology of the graph (e.g. bottlenecks), or it can be even 0 if two nodes are not connected by any walk. However, if the local sensitivity converges to 0, in the deep regime of large $t - s$, for all the pairs of nodes, i.e., if the global sensitivity converges to 0 regardless of the particular topology of the graph, then it means that the MPNN model is characterized by a vanishing information flow. Therefore, **lower bounds on global sensitivity are linked to the alleviation of vanishing gradient issues, in the deep regime**.

For connected graphs, we can leverage the exact Jacobian computation of Theorem 3.4 to prove the following lower bound on the global sensitivity, see Appendix A.5 for the proof.

Theorem 3.11 (Lower bound global sensitivity). *Assume a connected graph. The global sensitivity of the linear recurrent equation of an MP-SSM block is lower bounded as follows:*

$$\frac{\rho(\mathbf{A})^{t-s}}{|V|} \|\mathbf{W}^{t-s}\| \leq \mathcal{S}(t - s), \quad (10)$$

where $\rho(\mathbf{A})$ is the spectral radius of the GSO. Thus, for the GSO of Equation (1), it holds the lower bound $\frac{1}{|V|} \|\mathbf{W}^{t-s}\| \leq \mathcal{S}(t - s)$.

This theoretical result demonstrates that MP-SSM ensures values of the global sensitivity strictly greater than zero, for any depth $t - s$ and for connected graphs with any number of nodes. This result cannot be guaranteed in a standard MPNN, as the nonlinearity applied at each time step increasingly contributes to vanish information as the depth increases. We provide an extended discussion about this point in Appendix G.

Remark 3.12. Note that both results of Equation (6) and Equation (10) hold for any GSO. However, for the particular case of the symmetrically normalized adjacency with self-loops, we can provide more precise approximations and bounds.

From Section 2, we know that MP-SSM generalizes its backbone MPNNs, and the GCN architecture in particular when using Equation (1) as GSO. In Theorem 3.13, we provide an estimation of the vanishing effect caused by the application at each time step of a ReLU nonlinearity in a standard GCN compared with our MP-SSM, in the deep regime, as we prove in Appendix A.6.

Theorem 3.13 (GCN vanishes more than MP-SSM). *Let us consider a GCN network that aggregates information from k hops away, i.e., with k layers, equipped with the ReLU activation function. Then, the GCN vanishes information at a $2^{-\frac{k}{2}}$ faster rate than our MP-SSM block with k linear recurrent steps.*

4 Experiments

We evaluate MP-SSM on standard benchmarks for both static and temporal graphs. For static graphs, we assess long-range propagation via synthetic shortest-path tasks (Section 4.1) and heterophilic

node classification (Section 4.2). For temporal graphs, we test spatio-temporal forecasting performance (Section 4.3). Additionally, we benchmark MP-SSM on long-range real-world benchmarks in Appendix I. MP-SSM is compared against state-of-the-art MPNNs, multi-hop GNNs, graph transformers, graph SSMs, and spatio-temporal models (details in Appendix H.1). The closest baselines are MPNNs and graph SSMs. Hyperparameter settings are described in Appendix H.3. Code will be released upon acceptance. We emphasize that, unlike most state-of-the-art graph models, MP-SSM runs at a speed comparable to that of a standard GCN (see runtime and complexity analyses in Appendix F)—even without leveraging the optimized implementation discussed in Appendix B.

4.1 Graph Property Prediction

Setup. We evaluate MP-SSM on three synthetic tasks from [43]: predicting graph diameter, single-source shortest paths (SSSP), and node eccentricity. These tasks require long-range information flow, making them suitable benchmarks for evaluating propagation depth. We follow the original setup, data, and hyperparameters.

Results. Table 1 reports results using $\log_{10}(\text{MSE})$. MP-SSM outperforms all baselines, with an average gain of 2.4 points. On the eccentricity task, it improves over A-DGN by 3.4 points—despite A-DGN being tailored for long-range tasks—and exceeds GCN (its backbone model) by over 4 points on average, despite both using the same GSO. This highlights MP-SSM’s superior ability to propagate information across distant nodes.

4.2 Heterophilic Benchmark

Setup. We evaluate MP-SSM on five heterophilic benchmarks from [86]: Roman-empire, Amazon-ratings, Minesweeper, Tolokers, and Questions. These tasks test the model’s ability to capture complex interactions between dissimilar nodes. We follow the original data and experimental settings.

Results. Table 2 shows that MP-SSM consistently performs well, achieving the highest average ranking across all tasks (see Appendix J). It improves GCN by up to 17% and surpasses transformer- and SSM-based GNNs, including methods tailored for heterophilic graphs—demonstrating strong adaptability to

Table 1: Mean test set $\log_{10}(\text{MSE})$ (↓) and std averaged on 4 random weight initializations on Graph Property Prediction tasks. The lower, the better. **First**, **second**, and **third** best results for each task are color-coded.

Model	Diameter	SSSP	Eccentricity
MPNNs			
A-DGN	-0.5188\pm0.1812	-3.2417\pm0.0751	0.4296\pm0.1003
DGC	0.6028 \pm 0.0050	-0.1483 \pm 0.0231	0.8261 \pm 0.0032
GAT	0.8221 \pm 0.0752	0.6951 \pm 0.1499	0.7909 \pm 0.0222
GCN	0.7424 \pm 0.0466	0.9499 \pm 0.0001	0.8468 \pm 0.0028
GCNII	0.5287 \pm 0.0570	-1.1329 \pm 0.0135	0.7640 \pm 0.0355
GIN	0.6131 \pm 0.0990	-0.5408 \pm 0.4193	0.9504 \pm 0.0007
GRAND	0.6715 \pm 0.0490	-0.0942 \pm 0.3897	0.6602 \pm 0.1393
GraphCON	0.0964 \pm 0.0620	-1.3836 \pm 0.0092	0.6833 \pm 0.0074
GraphSAGE	0.8645 \pm 0.0401	0.2863 \pm 0.1843	0.7863 \pm 0.0207
Transformers			
GPS	-0.5121\pm0.0426	-3.5990\pm0.1949	0.6077\pm0.0282
Ours			
MP-SSM	-3.2353\pm0.1735	-4.6321\pm0.0779	-2.9724\pm0.0271

Table 2: Mean test set score and std averaged over 4 random weight initializations on heterophilic tasks. **First**, **second**, and **third** best results.

Model	Roman-empire	Amazon-ratings	Minesweep.	Tolokers	Questions
	Acc ↑	Acc ↑	AUC ↑	AUC ↑	AUC ↑
MPNNs					
CO-GNN	91.57\pm0.32	54.17\pm0.37	97.31\pm0.41	84.45\pm1.17	80.02\pm0.86
GAT	80.87 \pm 0.30	49.09 \pm 0.63	92.01 \pm 0.68	83.70 \pm 0.47	77.43 \pm 1.20
Gated-GCN	74.46 \pm 0.54	43.00 \pm 0.32	87.54 \pm 1.22	77.31 \pm 1.14	76.61 \pm 1.13
GCN	73.69 \pm 0.74	48.70 \pm 0.63	89.75 \pm 0.52	83.64 \pm 0.67	76.09 \pm 1.27
SAGE	85.74 \pm 0.67	53.63 \pm 0.39	93.51\pm0.57	82.43 \pm 0.44	76.44 \pm 0.62
Graph Transformers					
Exphormer	89.03\pm0.37	53.51 \pm 0.46	90.74 \pm 0.53	83.77 \pm 0.78	73.94 \pm 1.06
GOAT	71.59 \pm 1.25	44.61 \pm 0.50	81.09 \pm 1.02	83.11 \pm 1.04	75.76 \pm 1.66
GPS	82.00 \pm 0.61	53.10 \pm 0.42	90.63 \pm 0.67	83.71 \pm 0.48	71.73 \pm 1.47
GT	86.51 \pm 0.73	51.17 \pm 0.66	91.85 \pm 0.76	83.23 \pm 0.64	77.95 \pm 0.68
Heterophily-Designated GNNs					
FAGCN	65.22 \pm 0.56	44.12 \pm 0.30	88.17 \pm 0.73	77.75 \pm 1.05	77.24 \pm 1.26
FSGNN	79.92 \pm 0.56	52.74 \pm 0.83	90.08 \pm 0.70	82.76 \pm 0.61	78.86\pm0.92
GBK-GNN	74.57 \pm 0.47	45.98 \pm 0.71	90.85 \pm 0.58	81.01 \pm 0.67	74.47 \pm 0.86
GPR-GNN	64.85 \pm 0.27	44.88 \pm 0.34	86.24 \pm 0.61	72.94 \pm 0.97	55.48 \pm 0.91
H2GCN	60.11 \pm 0.52	36.47 \pm 0.23	89.71 \pm 0.31	73.35 \pm 1.01	63.59 \pm 1.46
Graph SSMs					
GMN	87.69 \pm 0.50	54.07\pm0.31	91.01 \pm 0.23	84.52\pm0.21	—
GPS+Mamba	83.10 \pm 0.28	45.13 \pm 0.97	89.93 \pm 0.54	83.70 \pm 1.05	—
Ours					
MP-SSM	90.91\pm0.48	53.65\pm0.71	95.33\pm0.72	85.26\pm0.93	78.18\pm1.34

complex, non-homophilic structures.

4.3 Spatio-Temporal Forecasting

Setup. We evaluate MP-SSM on five forecasting datasets: Metr-LA, PeMS-Bay [68], Chickenpox Hungary, PedalMe London, and Wikipedia math [89].

The goal is to predict future node values from time-series data. The first two focus on traffic, while the others involve public health, delivery demand, and web activity. We follow the original settings for each dataset.

Results. MP-SSM outperforms existing temporal GNNs across all datasets (Tables 3 and 4), highlighting its ability to model both spatial and temporal dependencies. These results confirm MP-SSM’s versatility across static and temporal graph domains. Notably, MP-SSM significantly outperforms GGRNN [90] and GraphSSM [66], see Table 4, two related state-space approaches for temporal graphs, thus highlighting the originality and effectiveness of our approach (see Appendix C for an extended discussion).

Table 3: Average MSE and standard deviation (\downarrow) of 10 experimental repetitions. Baseline results are reported from [89, 35, 34]. **First**, **second**, and **third** best methods for each task are color-coded.

Model	Chickenpox Hungary	PedalMe London	Wikipedia Math
Temporal GNNs			
A3T-GCN	1.114 ± 0.008	1.469 ± 0.027	0.781 ± 0.011
AGCRN	1.120 ± 0.010	1.469 ± 0.030	0.788 ± 0.011
CDE	0.848 ± 0.020	0.810 ± 0.063	0.694 ± 0.028
DCRNN	1.124 ± 0.015	1.463 ± 0.019	0.679 ± 0.020
DyGrAE	1.120 ± 0.021	1.455 ± 0.031	0.773 ± 0.009
DynGESN	0.907 ± 0.007	1.528 ± 0.063	0.610 ± 0.003
EGCN-O	1.124 ± 0.009	1.491 ± 0.024	0.750 ± 0.014
GConvGRU	1.128 ± 0.011	1.622 ± 0.032	0.657 ± 0.015
GC-LSTM	1.115 ± 0.014	1.455 ± 0.023	0.779 ± 0.023
GRAND	1.068 ± 0.021	1.557 ± 0.049	0.798 ± 0.034
GREAD	0.983 ± 0.027	1.291 ± 0.055	0.704 ± 0.016
HMM4G	0.939 ± 0.013	1.769 ± 0.370	0.542 ± 0.008
MPNN LSTM	1.116 ± 0.023	1.485 ± 0.028	0.795 ± 0.010
TDE-GNN	0.787 ± 0.018	0.714 ± 0.051	0.565 ± 0.017
T-GCN	1.117 ± 0.011	1.479 ± 0.012	0.764 ± 0.011
Ours			
MP-SSM	0.748 ± 0.011	0.647 ± 0.062	0.509 ± 0.008

5 Related Works

Learning Long-Range Dependencies on Graphs. While GNNs effectively model local structures via message passing, they struggle with long-range dependencies due to over-squashing and vanishing gradients [2, 27]. Standard models like GCN [61], GraphSAGE [50], and GIN [117] suffer from degraded performance on tasks requiring global context [5, 32], especially in heterophilic graphs [72, 111]. Solutions include graph rewiring [105, 60], weight-space regularization [43, 44], and physics-inspired dynamics [54]. Graph Transformers (GTs) like SAN [64], Graphomer [118], and GPS [88] enhance expressivity using structural encodings [33, 31], but suffer from quadratic complexity. Scalable alternatives include sparse and linearized attention mechanisms [119, 21, 96, 114, 26], though simple MPNNs often remain competitive [104].

Learning Spatio-Temporal Interactions on Graphs. Temporal GNNs often combine GNNs with RNNs to model spatio-temporal dynamics [42]. Some adopt stacked architectures that separate spatial and temporal processing [92, 83, 82, 6, 22], while others integrate GNNs within RNNs for joint modeling [65, 17, 68, 23, 90]. Our approach follows the latter, but goes further by embedding modern SSM principles directly into the GNN architecture, unifying spatial and temporal reasoning through linear recurrence. This contrasts with GGRNN [90], which employs a more elaborate message-passing scheme involving nonlinear aggregation over multiple powers of the graph shift operator at each recurrent step.

Casting State-Space Models into Graph Learning. Several recent models adopt SSMs for static graphs by imposing sequential orderings, e.g., via degree-based sorting [110] or random walks [10], often sacrificing permutation-equivariance. Spectral methods [57] offer alternatives but are computationally demanding and prone to over-squashing [27]. In the temporal graph setting, GraphSSM [66] applies the diffusive dynamics of a GNN backbone first, followed by an SSM as a post-processing module. In contrast, our approach embeds the core principles of modern SSMs directly into the graph learning process, yielding a unified framework that seamlessly supports both

Table 4: Multivariate time series forecasting on the Metr-LA and PeMS-Bay datasets for Horizon 12. **First**, **second**, and **third** best results for each task are color-coded. Baseline results are reported from [94, 70, 39, 36, 120].

Model	Metr-LA			PeMS-Bay		
	MAE ↓	RMSE ↓	MAPE ↓	MAE ↓	RMSE ↓	MAPE ↓
Graph Agnostic						
HA	6.99	13.89	17.54%	3.31	7.54	7.65%
FC-LSTM	4.37	8.69	14.00%	2.37	4.96	5.70%
SVR	6.72	13.76	16.70%	3.28	7.08	8.00%
VAR	6.52	10.11	15.80%	2.93	5.44	6.50%
Temporal GNNs						
AdpSTGCN	3.40	7.21	9.45%	1.92	4.49	4.62%
ASTGCN	6.51	12.52	11.64%	2.61	5.42	6.00%
DCRNN	3.60	7.60	10.50%	2.07	4.74	4.90%
GMAN	3.44	7.35	10.07%	1.86	4.32	4.37%
Graph WaveNet	3.53	7.37	10.01%	1.95	4.52	4.63%
GTS	3.46	7.31	9.98%	1.95	4.43	4.58%
MTGNN	3.49	7.23	9.87%	1.94	4.49	4.53%
RGDAN	3.26	7.02	9.73%	1.82	4.20	4.28%
STAEformer	3.34	7.02	9.70%	1.88	4.34	4.41%
STD-MAE	3.40	7.07	9.59%	1.77	4.20	4.17%
STEP	3.37	6.99	9.61%	1.79	4.20	4.18%
STGCN	4.59	9.40	12.70%	2.49	5.69	5.79%
STSGCN	5.06	11.66	12.91%	2.26	5.21	5.40%
Temporal Graph SSMs						
GGRNN	3.88	8.14	10.59%	2.34	5.14	5.21%
GraphSSM-S4	3.74	7.90	10.37%	1.98	4.45	4.77%
Ours						
MP-SSM	3.17	6.86	9.21%	1.62	4.22	4.05%

static and temporal graph modeling—while maintaining permutation equivariance, computational efficiency, and supporting parallel implementation.

6 Conclusions

We proposed the Message-Passing State-Space Model (MP-SSM), a novel framework that integrates state-space principles into MPNNs for effective and stable information propagation, while preserving graph topology and permutation-equivariance. MP-SSM supports exact sensitivity analysis and applies broadly to both static and temporal graphs. MP-SSM leverages on SSM principles that allow for a fast implementation. Extensive experiments across synthetic, long-range, heterophilic, and spatiotemporal tasks demonstrate its strong performance and theoretical soundness, positioning MP-SSM as a versatile and robust model for graph learning.

Impact Statement. This work aims to advance the field of machine learning on graph-structured data which are abundant in the real world. There are many potential societal consequences of our work, none which we feel must be specifically highlighted here.

References

- [1] Sami Abu-El-Haija, Bryan Perozzi, Amol Kapoor, Nazanin Alipourfard, Kristina Lerman, Hrayr Harutyunyan, Greg Ver Steeg, and Aram Galstyan. Mixhop: Higher-order graph convolutional architectures via sparsified neighborhood mixing. In *International Conference on Machine Learning*, pages 21–29. PMLR, 2019.
- [2] Uri Alon and Eran Yahav. On the bottleneck of graph neural networks and its practical implications. In *International Conference on Learning Representations*, 2021.

- [3] Álvaro Arroyo, Alessio Gravina, Benjamin Gutteridge, Federico Barbero, Claudio Gallicchio, Xiaowen Dong, Michael Bronstein, and Pierre Vandergheynst. On Vanishing Gradients, Over-Smoothing, and Over-Squashing in GNNs: Bridging Recurrent and Graph Learning. *arXiv preprint arXiv:2502.10818*, 2025.
- [4] Davide Bacci, Antonio Carta, and Alessandro Sperduti. Linear memory networks. In Igor V. Tetko, Věra Kůrková, Pavel Karpov, and Fabian Theis, editors, *Artificial Neural Networks and Machine Learning – ICANN 2019: Theoretical Neural Computation*, pages 513–525. Springer International Publishing, 2019.
- [5] Minkyung Baek, Frank DiMaio, Ivan Anishchenko, Justas Dauparas, Sergey Ovchinnikov, Gyu Rie Lee, Jue Wang, Qian Cong, Lisa N Kinch, R Dustin Schaeffer, et al. Accurate prediction of protein structures and interactions using a three-track neural network. *Science*, 373(6557):871–876, 2021.
- [6] Jiandong Bai, Jiawei Zhu, Yujiao Song, Ling Zhao, Zhixiang Hou, Ronghua Du, and Haifeng Li. A3T-GCN: Attention Temporal Graph Convolutional Network for Traffic Forecasting. *ISPRS International Journal of Geo-Information*, 10(7), 2021.
- [7] Lei Bai, Lina Yao, Can Li, Xianzhi Wang, and Can Wang. Adaptive graph convolutional recurrent network for traffic forecasting. In *Proceedings of the 34th International Conference on Neural Information Processing Systems*, NIPS ’20. Curran Associates Inc., 2020.
- [8] Anirban Banerjee and Ranjit Mehatari. An eigenvalue localization theorem for stochastic matrices and its application to randić matrices. *Linear Algebra and its Applications*, 505:85–96, 2016.
- [9] Maximilian Beck, Korbinian Pöppel, Markus Spanring, Andreas Auer, Oleksandra Prudnikova, Michael Kopp, Günter Klambauer, Johannes Brandstetter, and Sepp Hochreiter. xlstm: Extended long short-term memory. *arXiv preprint arXiv:2405.04517*, 2024.
- [10] Ali Behrouz and Farnoosh Hashemi. Graph mamba: Towards learning on graphs with state space models. In *Proceedings of the 30th ACM SIGKDD Conference on Knowledge Discovery and Data Mining*, pages 119–130, 2024.
- [11] Filippo Maria Bianchi, Daniele Grattarola, Lorenzo Livi, and Cesare Alippi. Graph neural networks with convolutional arma filters. *IEEE transactions on pattern analysis and machine intelligence*, 44(7):3496–3507, 2021.
- [12] Deyu Bo, Xiao Wang, Chuan Shi, and Huawei Shen. Beyond low-frequency information in graph convolutional networks. *Proceedings of the AAAI Conference on Artificial Intelligence*, 35(5):3950–3957, May 2021.
- [13] Xavier Bresson and Thomas Laurent. Residual Gated Graph ConvNets. *arXiv preprint arXiv:1711.07553*, 2018.
- [14] Michael M Bronstein, Joan Bruna, Taco Cohen, and Petar Veličković. Geometric deep learning: Grids, groups, graphs, geodesics, and gauges. *arXiv preprint arXiv:2104.13478*, 2021.
- [15] Benjamin Paul Chamberlain, James Rowbottom, Maria Gorinova, Stefan Webb, Emanuele Rossi, and Michael M Bronstein. GRAND: Graph neural diffusion. In *International Conference on Machine Learning (ICML)*, pages 1407–1418. PMLR, 2021.
- [16] Jinsong Chen, Kaiyuan Gao, Gaichao Li, and Kun He. NAGphormer: A tokenized graph transformer for node classification in large graphs. In *The Eleventh International Conference on Learning Representations*, 2023.
- [17] Jinyin Chen, Xueke Wang, and Xuanheng Xu. GC-LSTM: graph convolution embedded LSTM for dynamic network link prediction. *Applied Intelligence*, 52(7):7513–7528, May 2022.
- [18] Ming Chen, Zhewei Wei, Zengfeng Huang, Bolin Ding, and Yaliang Li. Simple and Deep Graph Convolutional Networks. In Hal Daumé III and Aarti Singh, editors, *Proceedings of the 37th International Conference on Machine Learning*, volume 119 of *Proceedings of Machine Learning Research*, pages 1725–1735. PMLR, 13–18 Jul 2020.

- [19] Eli Chien, Jianhao Peng, Pan Li, and Olgica Milenkovic. Adaptive universal generalized pagerank graph neural network. In *International Conference on Learning Representations*, 2021.
- [20] Jeongwhan Choi, Seoyoung Hong, Noseong Park, and Sung-Bae Cho. Gread: graph neural reaction-diffusion networks. In *Proceedings of the 40th International Conference on Machine Learning*, ICML'23. JMLR.org, 2023.
- [21] Krzysztof Choromanski, Marcin Kuczynski, Jacek Cieszkowski, Paul L. Beletsky, Konrad M. Smith, Wojciech Gajewski, Gabriel De Masson, Tomasz Z. Broniatowski, Antonina B. Gorny, Leszek M. Kaczmarek, and Stanislaw K. Andrzejewski. Performers: A new approach to scaling transformers. *Proceedings of the 37th International Conference on Machine Learning (ICML)*, pages 2020–2031, 2020.
- [22] A. Cini, I. Marisca, F.M. Bianchi, and C. Alippi. Scalable Spatiotemporal Graph Neural Networks. In *Proceedings of the AAAI Conference on Artificial Intelligence*, 2023.
- [23] Andrea Cini, Ivan Marisca, Daniele Zambon, and Cesare Alippi. Taming local effects in graph-based spatiotemporal forecasting. In A. Oh, T. Naumann, A. Globerson, K. Saenko, M. Hardt, and S. Levine, editors, *Advances in Neural Information Processing Systems*, volume 36, pages 55375–55393. Curran Associates, Inc., 2023.
- [24] Joni Dambre, David Verstraeten, Benjamin Schrauwen, and Serge Massar. Information processing capacity of dynamical systems. *Scientific reports*, 2(1):514, 2012.
- [25] Soham De, Samuel L Smith, Anushan Fernando, Aleksandar Botev, George Cristian-Muraru, Albert Gu, Ruba Haroun, Leonard Berrada, Yutian Chen, Srivatsan Srinivasan, et al. Griffin: Mixing gated linear recurrences with local attention for efficient language models. *arXiv preprint arXiv:2402.19427*, 2024.
- [26] Chenhui Deng, Zichao Yue, and Zhiru Zhang. Polynormer: Polynomial-expressive graph transformer in linear time. In *The Twelfth International Conference on Learning Representations*, 2024.
- [27] Francesco Di Giovanni, Lorenzo Giusti, Federico Barbero, Giulia Luise, Pietro Lio, and Michael M Bronstein. On over-squashing in message passing neural networks: The impact of width, depth, and topology. In *International Conference on Machine Learning*, pages 7865–7885. PMLR, 2023.
- [28] Yuhui Ding, Antonio Orvieto, Bobby He, and Thomas Hofmann. Recurrent distance filtering for graph representation learning. In *Forty-first International Conference on Machine Learning*, 2024.
- [29] Lun Du, Xiaozhou Shi, Qiang Fu, Xiaojun Ma, Hengyu Liu, Shi Han, and Dongmei Zhang. Gbk-gnn: Gated bi-kernel graph neural networks for modeling both homophily and heterophily. In *Proceedings of the ACM Web Conference 2022*, WWW '22, page 1550–1558, New York, NY, USA, 2022. Association for Computing Machinery.
- [30] Vijay Prakash Dwivedi and Xavier Bresson. A Generalization of Transformer Networks to Graphs. *AAAI Workshop on Deep Learning on Graphs: Methods and Applications*, 2021.
- [31] Vijay Prakash Dwivedi, Anh Tuan Luu, Thomas Laurent, Yoshua Bengio, and Xavier Bresson. Graph neural networks with learnable structural and positional representations. In *International Conference on Learning Representations*, 2022.
- [32] Vijay Prakash Dwivedi, Ladislav Rampášek, Michael Galkin, Ali Parviz, Guy Wolf, Anh Tuan Luu, and Dominique Beaini. Long range graph benchmark. *Advances in Neural Information Processing Systems*, 35:22326–22340, 2022.
- [33] Vishwajeet Dwivedi, Xavier Bresson, and Lior Wolf. Benchmarking graph neural networks. *Proceedings of the International Conference on Learning Representations (ICLR)*, 2021.

- [34] Moshe Eliasof, Eldad Haber, Eran Treister, and Carola-Bibiane B Schönlieb. On the temporal domain of differential equation inspired graph neural networks. In Sanjoy Dasgupta, Stephan Mandt, and Yingzhen Li, editors, *Proceedings of The 27th International Conference on Artificial Intelligence and Statistics*, volume 238 of *Proceedings of Machine Learning Research*, pages 1792–1800. PMLR, 02–04 May 2024.
- [35] Federico Errica, Alessio Gravina, Davide Baci, and Alessio Micheli. Hidden markov models for temporal graph representation learning. In *Proceedings of the 31st European Symposium on Artificial Neural Networks, Computational Intelligence and Machine Learning (ESANN)*, 2023.
- [36] Jin Fan, Wenchao Weng, Hao Tian, Huifeng Wu, Fu Zhu, and Jia Wu. Rgdn: A random graph diffusion attention network for traffic prediction. *Neural Networks*, 172:106093, 2024.
- [37] Ben Finkelshtein, Xingyue Huang, Michael M. Bronstein, and Ismail Ilkan Ceylan. Cooperative Graph Neural Networks. In *Forty-first International Conference on Machine Learning*, 2024.
- [38] Daniel Y Fu, Tri Dao, Khaled K Saab, Armin W Thomas, Atri Rudra, and Christopher Ré. Hungry hungry hippos: Towards language modeling with state space models. *arXiv preprint arXiv:2212.14052*, 2022.
- [39] Haotian Gao, Renhe Jiang, Zheng Dong, Jinliang Deng, Yuxin Ma, and Xuan Song. Spatial-temporal-decoupled masked pre-training for spatiotemporal forecasting. In *Proceedings of the Thirty-Third International Joint Conference on Artificial Intelligence, IJCAI '24*, 2024.
- [40] Johannes Gasteiger, Stefan Weiß enberger, and Stephan Günemann. Diffusion Improves Graph Learning. In *Advances in Neural Information Processing Systems*, volume 32. Curran Associates, Inc., 2019.
- [41] Gene H Golub and Charles F Van Loan. *Matrix computations*. JHU press, 2013.
- [42] Alessio Gravina and Davide Baci. Deep learning for dynamic graphs: Models and benchmarks. *IEEE Transactions on Neural Networks and Learning Systems*, 35(9):11788–11801, 2024.
- [43] Alessio Gravina, Davide Baci, and Claudio Gallicchio. Anti-Symmetric DGN: a stable architecture for Deep Graph Networks. In *The Eleventh International Conference on Learning Representations*, 2023.
- [44] Alessio Gravina, Moshe Eliasof, Claudio Gallicchio, Davide Baci, and Carola-Bibiane Schönlieb. On oversquashing in graph neural networks through the lens of dynamical systems. In *The 39th Annual AAAI Conference on Artificial Intelligence*, 2025.
- [45] Albert Gu and Tri Dao. Mamba: Linear-time sequence modeling with selective state spaces. *arXiv preprint arXiv:2312.00752*, 2023.
- [46] Albert Gu, Karan Goel, and Christopher Ré. Efficiently modeling long sequences with structured state spaces. *arXiv preprint arXiv:2111.00396*, 2021.
- [47] Shengnan Guo, Youfang Lin, Ning Feng, Chao Song, and Huaiyu Wan. Attention based spatial-temporal graph convolutional networks for traffic flow forecasting. *Proceedings of the AAAI Conference on Artificial Intelligence*, 33(01):922–929, Jul. 2019.
- [48] Ankit Gupta, Albert Gu, and Jonathan Berant. Diagonal state spaces are as effective as structured state spaces. *Advances in Neural Information Processing Systems*, 35:22982–22994, 2022.
- [49] Benjamin Gutteridge, Xiaowen Dong, Michael M Bronstein, and Francesco Di Giovanni. Drew: Dynamically rewired message passing with delay. In *International Conference on Machine Learning*, pages 12252–12267. PMLR, 2023.
- [50] William L. Hamilton, Rex Ying, and Jure Leskovec. Inductive representation learning on large graphs. In *Proceedings of the 31st International Conference on Neural Information Processing Systems*, NIPS'17, page 1025–1035. Curran Associates Inc., 2017.

- [51] Simon Haykin. *Neural networks and learning machines, 3/E*. Pearson Education India, 2009.
- [52] Kaiming He, Xiangyu Zhang, Shaoqing Ren, and Jian Sun. Deep residual learning for image recognition. In *Proceedings of the IEEE conference on computer vision and pattern recognition*, pages 770–778, 2016.
- [53] Xiaoxin He, Bryan Hooi, Thomas Laurent, Adam Perold, Yann LeCun, and Xavier Bresson. A generalization of vit/mlp-mixer to graphs. In *Proceedings of the 40th International Conference on Machine Learning, ICML’23*, 2023.
- [54] Simon Heilig, Alessio Gravina, Alessandro Trenta, Claudio Gallicchio, and Davide Bacciu. Port-hamiltonian architectural bias for long-range propagation in deep graph networks. In *The Thirteenth International Conference on Learning Representations*, 2025.
- [55] Roger A Horn and Charles R Johnson. *Matrix analysis*. Cambridge university press, 2012.
- [56] Weihua Hu, Bowen Liu, Joseph Gomes, Marinka Zitnik, Percy Liang, Vijay Pande, and Jure Leskovec. Strategies for Pre-training Graph Neural Networks. In *International Conference on Learning Representations*, 2020.
- [57] Yinan Huang, Siqi Miao, and Pan Li. What can we learn from state space models for machine learning on graphs? *arXiv preprint arXiv:2406.05815*, 2024.
- [58] Masanobu Inubushi and Kazuyuki Yoshimura. Reservoir computing beyond memory–nonlinearity trade-off. *Scientific reports*, 7(1):10199, 2017.
- [59] Herbert Jaeger. Short term memory in echo state networks. 2001.
- [60] Kedar Karhadkar, Pradeep Kr. Banerjee, and Guido Montufar. FoSR: First-order spectral rewiring for addressing oversquashing in GNNs. In *The Eleventh International Conference on Learning Representations*, 2023.
- [61] T. Kipf and M. Welling. Semi-supervised classification with graph convolutional networks. *Proceedings of the International Conference on Learning Representations*, 2016.
- [62] Kezhi Kong, Juhai Chen, John Kirchenbauer, Renkun Ni, C. Bayan Bruss, and Tom Goldstein. GOAT: A global transformer on large-scale graphs. In Andreas Krause, Emma Brunskill, Kyunghyun Cho, Barbara Engelhardt, Sivan Sabato, and Jonathan Scarlett, editors, *Proceedings of the 40th International Conference on Machine Learning*, volume 202 of *Proceedings of Machine Learning Research*, pages 17375–17390. PMLR, 23–29 Jul 2023.
- [63] Devin Kreuzer, Dominique Beaini, Will Hamilton, Vincent Létourneau, and Prudencio Tossou. Rethinking graph transformers with spectral attention. *Advances in Neural Information Processing Systems*, 34:21618–21629, 2021.
- [64] Sven Kreuzer, Michael Reiner, and Stefan D. D. De Villiers. Sant: Structural attention networks for graphs. *Proceedings of the 38th International Conference on Machine Learning (ICML)*, 2021.
- [65] Jia Li, Zhichao Han, Hong Cheng, Jiao Su, Pengyun Wang, Jianfeng Zhang, and Lujia Pan. Predicting Path Failure In Time-Evolving Graphs. In *Proceedings of the 25th ACM SIGKDD International Conference on Knowledge Discovery & Data Mining*, page 1279–1289, New York, NY, USA, 2019. Association for Computing Machinery.
- [66] Jintang Li, Ruofan Wu, Xinzhou Jin, Boqun Ma, Liang Chen, and Zibin Zheng. State space models on temporal graphs: A first-principles study. *Advances in Neural Information Processing Systems*, 37:127030–127058, 2024.
- [67] Xiang Li, Renyu Zhu, Yao Cheng, Caihua Shan, Siqiang Luo, Dongsheng Li, and Weining Qian. Finding global homophily in graph neural networks when meeting heterophily. In Kamalika Chaudhuri, Stefanie Jegelka, Le Song, Csaba Szepesvari, Gang Niu, and Sivan Sabato, editors, *Proceedings of the 39th International Conference on Machine Learning*, volume 162 of *Proceedings of Machine Learning Research*, pages 13242–13256. PMLR, 17–23 Jul 2022.

- [68] Yaguang Li, Rose Yu, Cyrus Shahabi, and Yan Liu. Diffusion Convolutional Recurrent Neural Network: Data-Driven Traffic Forecasting. In *International Conference on Learning Representations*, 2018.
- [69] Derek Lim, Joshua David Robinson, Lingxiao Zhao, Tess Smidt, Suvrit Sra, Haggai Maron, and Stefanie Jegelka. Sign and basis invariant networks for spectral graph representation learning. In *The Eleventh International Conference on Learning Representations*, 2023.
- [70] Hangchen Liu, Zheng Dong, Renhe Jiang, Jiewen Deng, Jinliang Deng, Quanjun Chen, and Xuan Song. Spatio-temporal adaptive embedding makes vanilla transformer sota for traffic forecasting. In *Proceedings of the 32nd ACM International Conference on Information and Knowledge Management*, pages 4125–4129, 2023.
- [71] Zheng Lu, Chen Zhou, Jing Wu, Hao Jiang, and Songyue Cui and. Integrating granger causality and vector auto-regression for traffic prediction of large-scale wlans. *KSII Transactions on Internet and Information Systems*, 10(1):136–151, January 2016.
- [72] Sitao Luan, Chenqing Hua, Qincheng Lu, Liheng Ma, Lirong Wu, Xinyu Wang, Minkai Xu, Xiao-Wen Chang, Doina Precup, Rex Ying, Stan Z. Li, Jian Tang, Guy Wolf, and Stefanie Jegelka. The heterophilic graph learning handbook: Benchmarks, models, theoretical analysis, applications and challenges. *arXiv preprint arXiv:2407.09618*, 2024.
- [73] Liheng Ma, Chen Lin, Derek Lim, Adriana Romero-Soriano, Puneet K. Dokania, Mark Coates, Philip Torr, and Ser-Nam Lim. Graph inductive biases in transformers without message passing. In *Proceedings of the 40th International Conference on Machine Learning*, volume 202 of *Proceedings of Machine Learning Research*, pages 23321–23337. PMLR, 23–29 Jul 2023.
- [74] Sunil Kumar Maurya, Xin Liu, and Tsuyoshi Murata. Simplifying approach to node classification in graph neural networks. *Journal of Computational Science*, 62:101695, 2022.
- [75] Carl D Meyer. *Matrix analysis and applied linear algebra*. SIAM, 2023.
- [76] Alessio Micheli and Domenico Tortorella. Discrete-time dynamic graph echo state networks. *Neurocomputing*, 496:85–95, 2022.
- [77] Nicola Muca Cirone, Antonio Orvieto, Benjamin Walker, Cristopher Salvi, and Terry Lyons. Theoretical foundations of deep selective state-space models. *Advances in Neural Information Processing Systems*, 37:127226–127272, 2024.
- [78] Luis Müller, Mikhail Galkin, Christopher Morris, and Ladislav Rampášek. Attending to graph transformers. *Transactions on Machine Learning Research*, 2024.
- [79] Kenta Oono and Taiji Suzuki. Graph neural networks exponentially lose expressive power for node classification. *arXiv preprint arXiv:1905.10947*, 2019.
- [80] Antonio Orvieto, Soham De, Caglar Gulcehre, Razvan Pascanu, and Samuel L Smith. Universality of linear recurrences followed by non-linear projections: Finite-width guarantees and benefits of complex eigenvalues. In *Forty-first International Conference on Machine Learning*, 2024.
- [81] Antonio Orvieto, Samuel L Smith, Albert Gu, Anushan Fernando, Caglar Gulcehre, Razvan Pascanu, and Soham De. Resurrecting recurrent neural networks for long sequences. In *International Conference on Machine Learning*, pages 26670–26698. PMLR, 2023.
- [82] George Panagopoulos, Giannis Nikolentzos, and Michalis Vazirgiannis. Transfer Graph Neural Networks for Pandemic Forecasting. In *Proceedings of the 35th AAAI Conference on Artificial Intelligence*, 2021.
- [83] Aldo Pareja, Giacomo Domeniconi, Jie Chen, Tengfei Ma, Toyotaro Suzumura, Hiroki Kanezashi, Tim Kaler, Tao B. Schardl, and Charles E. Leiserson. EvolveGCN: Evolving Graph Convolutional Networks for Dynamic Graphs. In *Proceedings of the 34th AAAI Conference on Artificial Intelligence*, 2020.

- [84] Razvan Pascanu, Tomas Mikolov, and Yoshua Bengio. On the difficulty of training recurrent neural networks. In Sanjoy Dasgupta and David McAllester, editors, *Proceedings of the 30th International Conference on Machine Learning*, volume 28 of *Proceedings of Machine Learning Research*, pages 1310–1318, Atlanta, Georgia, USA, 17–19 Jun 2013. PMLR.
- [85] Vladas Pipiras and Murad S Taqqu. *Long-range dependence and self-similarity*, volume 45. Cambridge university press, 2017.
- [86] Oleg Platonov, Denis Kuznedelev, Michael Diskin, Artem Babenko, and Liudmila Prokhorenkova. A critical look at the evaluation of GNNs under heterophily: Are we really making progress? In *The Eleventh International Conference on Learning Representations*, 2023.
- [87] Michael Poli, Stefano Massaroli, Eric Nguyen, Daniel Y Fu, Tri Dao, Stephen Baccus, Yoshua Bengio, Stefano Ermon, and Christopher Ré. Hyena hierarchy: Towards larger convolutional language models. In *International Conference on Machine Learning*, pages 28043–28078. PMLR, 2023.
- [88] Ladislav Rampášek, Mikhail Galkin, Vijay Prakash Dwivedi, Anh Tuan Luu, Guy Wolf, and Dominique Beaini. Recipe for a General, Powerful, Scalable Graph Transformer. *Advances in Neural Information Processing Systems*, 35, 2022.
- [89] Benedek Rozemberczki, Paul Scherer, Yixuan He, George Panagopoulos, Alexander Riedel, Maria Astefanoaei, Oliver Kiss, Ferenc Beres, Guzman Lopez, Nicolas Collignon, and Rik Sarkar. PyTorch Geometric Temporal: Spatiotemporal Signal Processing with Neural Machine Learning Models. In *Proceedings of the 30th ACM International Conference on Information and Knowledge Management*, page 4564–4573, 2021.
- [90] Luana Ruiz, Fernando Gama, and Alejandro Ribeiro. Gated graph recurrent neural networks. *IEEE Transactions on Signal Processing*, 68:6303–6318, 2020.
- [91] T Konstantin Rusch, Ben Chamberlain, James Rowbottom, Siddhartha Mishra, and Michael Bronstein. Graph-coupled oscillator networks. In *International Conference on Machine Learning*, pages 18888–18909. PMLR, 2022.
- [92] Youngjoo Seo, Michaël Defferrard, Pierre Vandergheynst, and Xavier Bresson. Structured Sequence Modeling with Graph Convolutional Recurrent Networks. In *Neural Information Processing*, pages 362–373, Cham, 2018. Springer International Publishing.
- [93] Chao Shang, Jie Chen, and Jinbo Bi. Discrete graph structure learning for forecasting multiple time series. In *International Conference on Learning Representations*, 2021.
- [94] Zezhi Shao, Zhao Zhang, Fei Wang, and Yongjun Xu. Pre-training enhanced spatial-temporal graph neural network for multivariate time series forecasting. In *KDD '22: The 28th ACM SIGKDD Conference on Knowledge Discovery and Data Mining, Washington, DC, USA, August 14 - 18, 2022*, pages 1567–1577. ACM, 2022.
- [95] Yunsheng Shi, Zhengjie Huang, Shikun Feng, Hui Zhong, Wenjing Wang, and Yu Sun. Masked label prediction: Unified message passing model for semi-supervised classification. In Zhi-Hua Zhou, editor, *Proceedings of the Thirtieth International Joint Conference on Artificial Intelligence, IJCAI-21*, pages 1548–1554. International Joint Conferences on Artificial Intelligence Organization, 8 2021. Main Track.
- [96] Behzad Shirzad, Amir M. Rahmani, and Marzieh Aghaei. Exphormer: Sparse attention for graphs. *Proceedings of the 40th International Conference on Machine Learning (ICML)*, 2023.
- [97] Jimmy TH Smith, Andrew Warrington, and Scott W Linderman. Simplified state space layers for sequence modeling. *arXiv preprint arXiv:2208.04933*, 2022.
- [98] Alex J. Smola and Bernhard Schölkopf. A tutorial on support vector regression. *Statistics and Computing*, 14(3):199–222, Aug 2004.

- [99] Chao Song, Youfang Lin, Shengnan Guo, and Huaiyu Wan. Spatial-temporal synchronous graph convolutional networks: A new framework for spatial-temporal network data forecasting. *Proceedings of the AAAI Conference on Artificial Intelligence*, 34(01):914–921, Apr. 2020.
- [100] Nitish Srivastava, Geoffrey Hinton, Alex Krizhevsky, Ilya Sutskever, and Ruslan Salakhutdinov. Dropout: a simple way to prevent neural networks from overfitting. *The journal of machine learning research*, 15(1):1929–1958, 2014.
- [101] Ilya Sutskever, Oriol Vinyals, and Quoc V. Le. Sequence to sequence learning with neural networks. In *Proceedings of the 28th International Conference on Neural Information Processing Systems*, volume 2 of *NIPS’14*, page 3104–3112, Cambridge, MA, USA, 2014. MIT Press.
- [102] Aynaz Taheri and Tanya Berger-Wolf. Predictive temporal embedding of dynamic graphs. In *Proceedings of the 2019 IEEE/ACM International Conference on Advances in Social Networks Analysis and Mining*, ASONAM ’19, page 57–64. Association for Computing Machinery, 2020.
- [103] Siyi Tang, Jared A Dunnmon, Qu Liangqiong, Khaled K Saab, Tina Baykaner, Christopher Lee-Messer, and Daniel L Rubin. Modeling multivariate biosignals with graph neural networks and structured state space models. In *Conference on Health, Inference, and Learning*, pages 50–71. PMLR, 2023.
- [104] Jan Tönshoff, Martin Ritzert, Eran Rosenbluth, and Martin Grohe. Where did the gap go? reassessing the long-range graph benchmark. In *The Second Learning on Graphs Conference*, 2023.
- [105] Matthew Topping, Sebastian Ruder, and Chris Dyer. Understanding over-smoothing in graph neural networks. *Proceedings of the 39th International Conference on Machine Learning (ICML)*, 2022.
- [106] A. Vaswani et al. Attention is all you need. *Advances in Neural Information Processing Systems*, 30, 2017.
- [107] Ashish Vaswani, Noam Shazeer, Niki Parmar, Jakob Uszkoreit, Llion Jones, Aidan N Gomez, Łukasz Kaiser, and Illia Polosukhin. Attention is all you need. *Advances in neural information processing systems*, 30, 2017.
- [108] Petar Veličković, Guillem Cucurull, Arantxa Casanova, Adriana Romero, Pietro Liò, and Yoshua Bengio. Graph attention networks. In *International Conference on Learning Representations*, 2018.
- [109] Aaron Voelker, Ivana Kajić, and Chris Eliasmith. Legendre memory units: Continuous-time representation in recurrent neural networks. *Advances in neural information processing systems*, 32, 2019.
- [110] Chloe Wang, Oleksii Tsepa, Jun Ma, and Bo Wang. Graph-mamba: Towards long-range graph sequence modeling with selective state spaces. *arXiv preprint arXiv:2402.00789*, 2024.
- [111] Kun Wang, Guibin Zhang, Xinnan Zhang, Junfeng Fang, Xun Wu, Guohao Li, Shirui Pan, Wei Huang, and Yuxuan Liang. The heterophilic snowflake hypothesis: Training and empowering gnns for heterophilic graphs. In *Proceedings of the 30th ACM SIGKDD Conference on Knowledge Discovery and Data Mining*, KDD ’24, page 3164–3175, New York, NY, USA, 2024. Association for Computing Machinery.
- [112] Xiyuan Wang and Muhan Zhang. How powerful are spectral graph neural networks. In Kamalika Chaudhuri, Stefanie Jegelka, Le Song, Csaba Szepesvari, Gang Niu, and Sivan Sabato, editors, *Proceedings of the 39th International Conference on Machine Learning*, volume 162 of *Proceedings of Machine Learning Research*, pages 23341–23362. PMLR, 17–23 Jul 2022.
- [113] Yifei Wang, Yisen Wang, Jiansheng Yang, and Zhouchen Lin. Dissecting the Diffusion Process in Linear Graph Convolutional Networks. In *Advances in Neural Information Processing Systems*, volume 34, pages 5758–5769. Curran Associates, Inc., 2021.

- [114] Yi Wu, Yanyang Xu, Wenhao Zhu, Guojie Song, Zhouchen Lin, Liang Wang, and Shaoguo Liu. Kdlgt: A linear graph transformer framework via kernel decomposition approach. In *IJCAI*, pages 2370–2378, 2023.
- [115] Zonghan Wu, Shirui Pan, Guodong Long, Jing Jiang, Xiaojun Chang, and Chengqi Zhang. Connecting the dots: Multivariate time series forecasting with graph neural networks. In *Proceedings of the 26th ACM SIGKDD International Conference on Knowledge Discovery & Data Mining, KDD '20*, page 753–763, New York, NY, USA, 2020. Association for Computing Machinery.
- [116] Zonghan Wu, Shirui Pan, Guodong Long, Jing Jiang, and Chengqi Zhang. Graph wavenet for deep spatial-temporal graph modeling. In *Proceedings of the 28th International Joint Conference on Artificial Intelligence, IJCAI'19*, page 1907–1913. AAAI Press, 2019.
- [117] Keyulu Xu, Weihua Hu, Jure Leskovec, and Stefanie Jegelka. How powerful are graph neural networks? In *International Conference on Learning Representations*, 2019.
- [118] Zhitao Ying and Jure Leskovec. Graphomer: A transformer for graphs. *Proceedings of the 43rd International ACM SIGIR Conference on Research and Development in Information Retrieval*, 2021.
- [119] Manzil Zaheer, Guru prasad G. H., Lihong Wang, S. V. K. N. L. Wang, Yujia Li, Jakub Konečný, Shalmali Joshi, Danqi Chen, Jennifer R. R., Zhenyu Zhang, Shalini Devaraj, and Srinivas Narayanan. Bigbird: Transformers for longer sequences. *Proceedings of the 37th International Conference on Machine Learning (ICML)*, pages 12168–12178, 2020.
- [120] Xudong Zhang, Xuewen Chen, Haina Tang, Yulei Wu, Hanji Shen, and Jun Li. Adpstgcn: Adaptive spatial–temporal graph convolutional network for traffic forecasting. *Knowledge-Based Systems*, 301:112295, 2024.
- [121] Gongpei Zhao, Tao Wang, Yi Jin, Congyan Lang, Yidong Li, and Haibin Ling. Grassnet: State space model meets graph neural network. *arXiv preprint arXiv:2408.08583*, 2024.
- [122] Kai Zhao, Qiyu Kang, Yang Song, Rui She, Sijie Wang, and Wee Peng Tay. Graph neural convection-diffusion with heterophily. In Edith Elkind, editor, *Proceedings of the Thirty-Second International Joint Conference on Artificial Intelligence, IJCAI-23*, pages 4656–4664. International Joint Conferences on Artificial Intelligence Organization, 8 2023. Main Track.
- [123] Ling Zhao, Yujiao Song, Chao Zhang, Yu Liu, Pu Wang, Tao Lin, Min Deng, and Haifeng Li. T-GCN: A Temporal Graph Convolutional Network for Traffic Prediction. *IEEE Transactions on Intelligent Transportation Systems*, 21(9):3848–3858, 2020.
- [124] Chuanpan Zheng, Xiaoliang Fan, Cheng Wang, and Jianzhong Qi. Gman: A graph multi-attention network for traffic prediction. *Proceedings of the AAAI Conference on Artificial Intelligence*, 34(01):1234–1241, Apr. 2020.
- [125] Jiong Zhu, Ryan A. Rossi, Anup Rao, Tung Mai, Nedim Lipka, Nesreen K. Ahmed, and Danai Koutra. Graph neural networks with heterophily. *Proceedings of the AAAI Conference on Artificial Intelligence*, 35(12):11168–11176, May 2021.
- [126] Jiong Zhu, Yujun Yan, Lingxiao Zhao, Mark Heimann, Leman Akoglu, and Danai Koutra. Beyond homophily in graph neural networks: Current limitations and effective designs. In H. Larochelle, M. Ranzato, R. Hadsell, M.F. Balcan, and H. Lin, editors, *Advances in Neural Information Processing Systems*, volume 33, pages 7793–7804. Curran Associates, Inc., 2020.

A Proofs

Here, we provide all the proofs of lemmas, theorems, and corollaries stated in the main text.

A.1 Proof of Lemma 3.5

Lemma. Assume an undirected graph. The spectrum of the powers of the symmetric normalized adjacency matrix $\mathbf{A} = \mathbf{D}^{-\frac{1}{2}}(\tilde{\mathbf{A}} + \mathbf{I})\mathbf{D}^{-\frac{1}{2}}$ is contained in the interval $[-1, 1]$. The largest eigenvalue of \mathbf{A}^t has absolute value of 1 with corresponding eigenvector $\mathbf{d} = \text{diag}(\mathbf{D}^{\frac{1}{2}})$, for all $t \geq 1$. In particular, the sequence of powers $[\mathbf{A}^t]_{t \geq 1}$ does not diverge or converge to the null matrix.

Proof. $\mathbf{A}^t = (\mathbf{D}^{-\frac{1}{2}}(\tilde{\mathbf{A}} + \mathbf{I})\mathbf{D}^{-\frac{1}{2}})(\mathbf{D}^{-\frac{1}{2}}(\tilde{\mathbf{A}} + \mathbf{I})\mathbf{D}^{-\frac{1}{2}}) \dots (\mathbf{D}^{-\frac{1}{2}}(\tilde{\mathbf{A}} + \mathbf{I})\mathbf{D}^{-\frac{1}{2}}) = \mathbf{D}^{-\frac{1}{2}}(\tilde{\mathbf{A}} + \mathbf{I})(\mathbf{D}^{-1}(\tilde{\mathbf{A}} + \mathbf{I}))^{t-1}\mathbf{D}^{-\frac{1}{2}}$. Now, $\mathbf{D}^{-1}(\tilde{\mathbf{A}} + \mathbf{I})$ is a stochastic matrix, and so also its powers are stochastic matrices. Therefore, $\mathbf{D}^{-\frac{1}{2}}\mathbf{A}^t\mathbf{D}^{\frac{1}{2}} = (\mathbf{D}^{-1}(\tilde{\mathbf{A}} + \mathbf{I}))^t$ is a stochastic matrix. The eigenvalues of a stochastic matrix are contained in the closed unitary disk [75, 8]. Let, $\lambda_1, \dots, \lambda_n$ all the eigenvalues (not necessarily distinct) of such a stochastic matrix, with corresponding eigenvectors $\mathbf{v}_1, \dots, \mathbf{v}_n$. Thus, $\mathbf{D}^{-\frac{1}{2}}\mathbf{A}^t\mathbf{D}^{\frac{1}{2}}\mathbf{v}_l = \lambda_l\mathbf{v}_l$, from which it follows, multiplying both sides by $\mathbf{D}^{\frac{1}{2}}$, that $\mathbf{A}^t\mathbf{D}^{\frac{1}{2}}\mathbf{v}_l = \lambda_l\mathbf{D}^{\frac{1}{2}}\mathbf{v}_l$. This means that the eigenvalues of \mathbf{A}^t are exactly the same of those of the stochastic matrix $\mathbf{D}^{-\frac{1}{2}}\mathbf{A}^t\mathbf{D}^{\frac{1}{2}}$ with eigenvectors $\mathbf{D}^{\frac{1}{2}}\mathbf{v}_1, \dots, \mathbf{D}^{\frac{1}{2}}\mathbf{v}_n$, for all t . In particular, the assumption of undirected graph implies \mathbf{A} is a symmetric matrix, thus we get that all eigenvalues of \mathbf{A}^t are real and contained inside $[-1, 1]$, for all t . Since the spectral radius of a stochastic matrix is 1, and the vector $\mathbf{1}$ with all components equal to 1 is necessarily an eigenvector due to the row-sum being 1 for a stochastic matrix, then it follows that the largest eigenvalue of \mathbf{A}^t is 1 and $\mathbf{d} = \text{diag}(\mathbf{D}^{\frac{1}{2}})$ is an eigenvector corresponding to eigenvalue 1, for all t . To see why the sequence of powers $[\mathbf{A}^t]_{t \geq 1}$ does not diverge or converge to the null matrix, we observe that, since \mathbf{A} is symmetric, the Spectral Theorem implies we can diagonalize in \mathbb{R} the matrix $\mathbf{A} = \mathbf{Q}\Lambda\mathbf{Q}^\top$ with \mathbf{Q} orthogonal matrix and Λ diagonal matrix of real eigenvalues. Powers of \mathbf{A} can be written as $\mathbf{A}^t = (\mathbf{Q}\Lambda\mathbf{Q}^\top)(\mathbf{Q}\Lambda\mathbf{Q}^\top) \dots (\mathbf{Q}\Lambda\mathbf{Q}^\top) = \mathbf{Q}\Lambda^t\mathbf{Q}^\top$. Thus the eigenvalues of \mathbf{A}^t are λ_l^t , for $l = 1, \dots, n$. We already proved that the eigenvalues $\lambda_n \leq \dots \leq \lambda_1$ are contained in the real interval $[-1, 1]$. Hence, this ensures that the sequence of powers cannot diverge. On the other hand, we can spectrally decompose symmetric matrices as follows [51], $\mathbf{A}^t = \sum_{l=1}^n \lambda_l^t \mathbf{q}_l \mathbf{q}_l^\top$, where \mathbf{q}_l is the eigenvector corresponding to the eigenvalue λ_l . Thus, for large values of t , the spectral components corresponding to eigenvalues strictly less than 1 in absolute value vanish, so the matrix \mathbf{A}^t approaches the sum of terms corresponding to eigenvalues with absolute value equal to 1. This proves that the sequence of powers cannot converge to the null matrix. \square

A.2 Proof of Theorem 3.4

Theorem. The Jacobian of the linear recurrent equation of an MP-SSM block, from node j at layer s to node i at layer $t \geq s$, can be computed exactly, and it has the following form:

$$\frac{\partial \mathbf{X}_t^{(i)}}{\partial \mathbf{X}_s^{(j)}} = \underbrace{(\mathbf{A}^{t-s})_{ij}}_{\text{scalar}} \underbrace{(\mathbf{W}^\top)^{t-s}}_{\text{matrix}}.$$

Proof. In this proof we use the notation $(\mathbf{M})_{ij}$ to denote the (i, j) entry of a matrix \mathbf{M} , and $\mathbf{M}^{(i)}$ to denote the i -th row of a matrix \mathbf{M} . Let us start with the recurrent equation $\mathbf{X}_{t+1} = \mathbf{A}\mathbf{X}_t\mathbf{W} + \mathbf{U}_{t+1}\mathbf{B}$. Therefore, the i -th node features are updated as follows: $\mathbf{X}_{t+1}^{(i)} = \sum_{l=1}^n (\mathbf{A})_{il} \mathbf{X}_t^{(l)} \mathbf{W} + \mathbf{U}_{t+1}^{(i)} \mathbf{B}$. Now, the only term involving $\mathbf{X}_t^{(j)}$ is $(\mathbf{A})_{ij} \mathbf{X}_t^{(j)} \mathbf{W}$. Therefore, the Jacobian reads $\frac{\partial \mathbf{X}_{t+1}^{(i)}}{\partial \mathbf{X}_t^{(j)}} = \frac{\partial}{\partial \mathbf{X}_t^{(j)}} ((\mathbf{A})_{ij} \mathbf{X}_t^{(j)} \mathbf{W})$. Now, given a row vector $\mathbf{x} \in \mathbb{R}^c$ and a square matrix \mathbf{M} , then the function $\mathbf{f}(\mathbf{x}) = \mathbf{x}\mathbf{M}$, whose i -th component is $f_i = \sum_{l=1}^c x_l (\mathbf{M})_{li}$, has derivatives $\frac{\partial f_i}{\partial \mathbf{x}_j} = \frac{\partial}{\partial \mathbf{x}_j} (x_j (\mathbf{M})_{ji}) =$

$(\mathbf{M})_{ji}$. Hence, the Jacobian is $\frac{\partial \mathbf{f}}{\partial \mathbf{x}} = \mathbf{M}^\top$. Therefore, it holds $\frac{\partial \mathbf{X}_{t+1}^{(i)}}{\partial \mathbf{X}_t^{(j)}} = (\mathbf{A})_{ji} \mathbf{W}^\top$. For the case of non-consecutive time steps, we can unfold the recurrent equation $\mathbf{X}_{t+1} = \mathbf{A} \mathbf{X}_t \mathbf{W} + \mathbf{U}_{t+1} \mathbf{B}$ between any two time steps $s \leq t$, as follows:

$$\mathbf{X}_t = \mathbf{A}^{t-s} \mathbf{X}_s \mathbf{W}^{t-s} + \sum_{l=0}^{t-s-1} \mathbf{A}^l \mathbf{U}_{t-l} \mathbf{B} \mathbf{W}^i. \quad (11)$$

From the unfolded recurrent equation (11) of a MP-SSM we can see that the only term involving \mathbf{X}_s is $\mathbf{A}^{t-s} \mathbf{X}_s \mathbf{W}^{t-s}$. Thus, the Jacobian reads $\frac{\partial \mathbf{X}_t^{(i)}}{\partial \mathbf{X}_s^{(j)}} = \frac{\partial}{\partial \mathbf{X}_s^{(j)}} \left((\mathbf{A}^{t-s} \mathbf{X}_s \mathbf{W}^{t-s})^{(i)} \right) = \frac{\partial}{\partial \mathbf{X}_s^{(j)}} \left((\mathbf{A}^{t-s})_{ij} \mathbf{X}_s^{(j)} \mathbf{W}^{t-s} \right) = (\mathbf{A}^{t-s})_{ij} (\mathbf{W}^\top)^{t-s}$. \square

A.3 Proof of Theorem 3.6

Theorem. Assume a connected graph, and the GSO defined in Equation (1). Then, for large values of $t - s$, the Jacobian of the linear recurrent equation of an MP-SSM block, from node j at layer s to node i at layer $t \geq s$, admits the following approximation:

$$\frac{\partial \mathbf{X}_t^{(i)}}{\partial \mathbf{X}_s^{(j)}} \approx \frac{\sqrt{(1+d_i)(1+d_j)}}{|V| + 2|E|} (\mathbf{W}^\top)^{t-s},$$

where $d_l = \sum_{j=1}^n (\tilde{\mathbf{A}})_{lj}$ is the degree of the l -th node.

Proof. We provide an estimation of the term $(\mathbf{A}^{t-s})_{ij}$ for the case of large values of $t - s$, and assuming a connected graph. We use the decomposition $\mathbf{A}^{t-s} = \sum_{l=1}^n \lambda_l^{t-s} \mathbf{q}_l \mathbf{q}_l^\top$, where \mathbf{q}_l is the unitary eigenvector corresponding to the eigenvalue λ_l . As discussed in the proof of Lemma 3.5, for large values of $t - s$, all the spectral components corresponding to eigenvalues strictly less than 1 (in absolute value) tend to converge to 0. Moreover, by the Perron–Frobenius theorem for irreducible non-negative matrices [55], since the graph is connected and with self-loops, there is only one simple eigenvalue equal to 1, and -1 cannot be an eigenvalue. Thus it holds the approximation $\mathbf{A}^{t-s} \approx \mathbf{q}_1 \mathbf{q}_1^\top$. Now thanks to Lemma 3.5, we know that \mathbf{q}_1 must be the vector $\mathbf{d} = \text{diag}(\mathbf{D}^{\frac{1}{2}})$ normalised to be unitary, and \mathbf{D} is the degree matrix of $\tilde{\mathbf{A}} + \mathbf{I}$. Thus, $\mathbf{q}_1 = \frac{(\sqrt{1+d_1}, \dots, \sqrt{1+d_n})}{\sqrt{\sum_{l=1}^n (1+d_l)}}$, where $d_l = \sum_{j=1}^n (\tilde{\mathbf{A}})_{lj}$ is the degree of the l -th node. Therefore, $(\mathbf{q}_1 \mathbf{q}_1^\top)_{ij} = \frac{\sqrt{(1+d_i)(1+d_j)}}{n + \sum_{l=1}^n d_l} = \frac{\sqrt{(1+d_i)(1+d_j)}}{|V| + 2|E|}$. \square

A.3.1 Example of a bad scenario for Equation (7)

Figure 2 illustrates an example of a bad scenario for Equation (7), i.e., a chain of m cliques of order d connected via bridge-nodes of degree 2 (the minimum to connect them). In the Figure, we consider $m = 6$ and $d = 10$. The pair of bridge nodes i and j depicted in red in Figure 2 are 12 hops apart, so it can be considered a relatively long-term interaction.

In the long-term approximation given by Equation (7), the local sensitivity between two bridge nodes of this topology scales as $\frac{1}{md^2}$, for long chains (m large) and big cliques (d large). In fact, in such a graph the vast majority of nodes has degree approximately $d - 1$, thus $\sum_{l=1}^n d_l \approx n(d - 1)$. Specifically, there are exactly $m - 1$ nodes of degree 2 (bridge nodes), and md nodes with degree approximately $d - 1$. Now, $n = m - 1 + md \approx md$, therefore $n + \sum_{l=1}^n d_l \approx n + n(d - 1) = nd \approx md^2$. Scaling to long chains and large cliques, this approximation becomes more accurate, and so the local sensitivity between two bridge nodes is rescaled by the term $\frac{\sqrt{(1+d_i)(1+d_j)}}{n + \sum_{l=1}^n d_l} \approx \frac{3}{md^2}$.

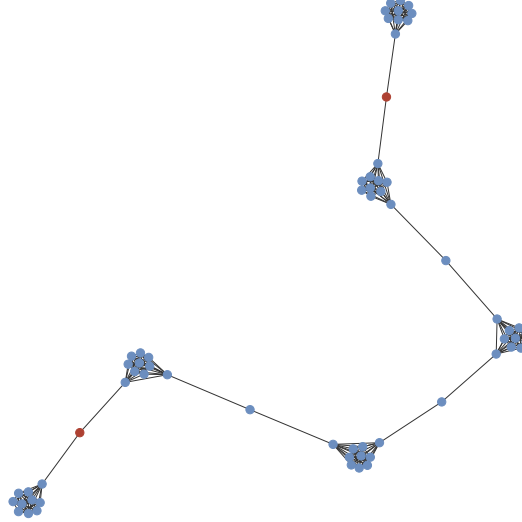


Figure 2: A chain of six cliques (containing ten nodes each) connected via bridge-nodes of degree 2. The pair of red nodes is a pair of nodes that minimizes the quantity in Equation (7). Note that the red nodes are 12 hops apart, so it can be considered long-term.

A.4 Proof of Corollary 3.7

Corollary. Assume a connected graph, and the GSO of Equation (1). Then, for large values of $t - s$, the following lower bound for the minimum local sensitivity of the linear recurrent equation of an MP-SSM block holds:

$$\frac{2}{|V| + 2|E|} \|\mathbf{W}^{t-s}\| \leq \min_{i,j} \mathcal{S}_{ij}(t-s). \quad (12)$$

Proof. In the deep regime, we can use the approximation of Equation (7) of $\frac{\partial \mathbf{X}_t^{(i)}}{\partial \mathbf{X}_s^{(j)}} \approx \frac{\sqrt{(1+d_i)(1+d_j)}}{|V|+2|E|} (\mathbf{W}^\top)^{t-s}$. Therefore, we have:

$$\min_{i,j} \left\| \frac{\partial \mathbf{X}_t^{(i)}}{\partial \mathbf{X}_s^{(j)}} \right\| \approx \frac{1}{|V| + 2|E|} \left\| (\mathbf{W}^\top)^{t-s} \right\| \min_{i,j} \sqrt{(1+d_i)(1+d_j)} \geq \frac{2}{|V| + 2|E|} \left\| (\mathbf{W}^\top)^{t-s} \right\|,$$

where the last inequality holds since the minimum degree value of a node in a connected graph is 1. Thus, we conclude that $\min_{i,j} \mathcal{S}_{ij}(t-s) \geq \frac{2}{|V| + 2|E|} \left\| (\mathbf{W}^\top)^{t-s} \right\| = \frac{2}{|V| + 2|E|} \|\mathbf{W}^{t-s}\|$, noticing that $\|\mathbf{W}^\top\| = \|\mathbf{W}\|$. \square

A.5 Proof of Theorem 3.11

Theorem. Assume a connected graph. The global sensitivity of the linear recurrent equation of an MP-SSM block is lower bounded as follows:

$$\mathcal{S}(t-s) \geq \frac{\rho(\mathbf{A})^{t-s}}{|V|} \|\mathbf{W}^{t-s}\|,$$

where $\rho(\mathbf{A})$ is the spectral radius of the GSO. Thus, for the GSO of Equation (1), it holds the lower bound $\mathcal{S}(t-s) \geq \frac{1}{|V|} \|\mathbf{W}^{t-s}\|$.

Proof. By Equations (5), (6) and (9), we get $\mathcal{S}(t-s) = \max_{i,j} |(\mathbf{A}^{t-s})_{ij}| \|\mathbf{W}^{t-s}\| = \max_{i,j} |(\mathbf{A}^{t-s})_{ij}| \|\mathbf{W}^{t-s}\|$. Let us define $n = |V|$ the number of nodes. The square of the maximum

entry of an (n, n) matrix \mathbf{M} is always greater than the arithmetic mean of all the square coefficients, in other words, $\frac{\|\mathbf{M}\|_F^2}{n^2} \leq \max_{i,j} \mathbf{M}_{i,j}^2$, where $\|\mathbf{M}\|_F$ denotes the Frobenius norm. Therefore, $\frac{\|\mathbf{M}\|_F}{n} \leq \max_{i,j} |\mathbf{M}_{i,j}|$. Now, the symmetry of \mathbf{A} implies there are $\lambda_1, \dots, \lambda_n$ real eigenvalues with corresponding orthonormal eigenvectors $\mathbf{q}_1, \dots, \mathbf{q}_n$ so that we can decompose $\mathbf{A}^{t-s} = \sum_{l=1}^n \lambda_l^{t-s} \mathbf{q}_l \mathbf{q}_l^\top$. Thus, the Frobenius norm is $\|\mathbf{A}^{t-s}\|_F = \sqrt{\sum_{l=1}^n \lambda_l^{2(t-s)}} \|\mathbf{q}_l\|^2 = \sqrt{\sum_{l=1}^n \lambda_l^{2(t-s)}} \geq |\lambda_1|^{t-s}$, where $|\lambda_1|$ is the largest in absolute value between all the eigenvalues, i.e. the spectral radius $\rho(\mathbf{A})$.

$$\max_{i,j} |(\mathbf{A}^{t-s})_{ij}| \geq \frac{\|\mathbf{A}^{t-s}\|_F}{n} \geq \frac{\rho(\mathbf{A})^{t-s}}{n}, \quad (13)$$

from which we get the thesis

$$\mathcal{S}(t-s) = \max_{i,j} |(\mathbf{A}^{t-s})_{ij}| \|\mathbf{W}^{t-s}\| \geq \frac{\rho(\mathbf{A})^{t-s}}{n} \|\mathbf{W}^{t-s}\|.$$

For the particular case of GSO given by Equation (1), the spectral radius $\rho(\mathbf{A})$ is exactly 1 due to Lemma 3.5. \square

A.6 Proof of Theorem 3.13

Theorem. Let us consider a GCN network that aggregates information from k hops away, i.e., with k layers, equipped with the ReLU activation function. Then, the GCN vanishes information at a $2^{-\frac{k}{2}}$ faster rate than our MP-SSM block with a number k of linear recurrent steps.

Proof. The state-update equation of a GCN with a residual connection is $\mathbf{X}_{t+1} = \sigma(\mathbf{A}\mathbf{X}_t\mathbf{W} + \mathbf{X}_t)$. Therefore, the features of i -th node at time $t+1$ are updated as $\mathbf{X}_{t+1}^{(i)} = \sigma\left(\sum_{l=1}^n (\mathbf{A})_{il} \mathbf{X}_t^{(l)} \mathbf{W} + \mathbf{X}_t^{(i)}\right)$. Similarly to the proof of theorem 3.4, we can write

$$\begin{aligned} \frac{\partial \mathbf{X}_{t+1}^{(i)}}{\partial \mathbf{X}_t^{(j)}} &= \frac{\partial}{\partial \mathbf{X}_t^{(j)}} \left(\sigma\left((\mathbf{A})_{ij} \mathbf{X}_t^{(j)} \mathbf{W}\right) \right) = \\ &= \text{diag}\left(\sigma'\left((\mathbf{A})_{ij} \mathbf{X}_t^{(j)} \mathbf{W}\right)\right) (\mathbf{A})_{ij} \mathbf{W}^\top, \end{aligned}$$

where we assumed that $i \neq j$, so that the residual connection term does not appear in the derivative w.r.t. $\mathbf{X}_t^{(j)}$. Since we are considering $\sigma = \text{ReLU}$, the diagonal entries $\sigma'\left((\mathbf{A})_{ij} \mathbf{X}_t^{(j)} \mathbf{W}\right)$ are either 0 or 1. Let's assume that the components of the vector $\sigma'\left((\mathbf{A})_{ij} \mathbf{X}_t^{(j)} \mathbf{W}\right)$ are independent and identically distributed (i.i.d.) Bernoulli random variables, each with probability $\frac{1}{2}$ of taking the value 0. Now, let's consider a walk $\{(i_t, j_t)\}_{t=0}^{k-1}$ of length k connecting the j -th node at a reference time $t = 0$ to the i -th node at time $t = k$. Then, the Jacobian of GCN along such a walk reads:

$$\frac{\partial \mathbf{X}_k^{(i)}}{\partial \mathbf{X}_0^{(j)}} = \prod_{t=0}^{k-1} \mathbf{P}_t \mathbf{M}_t,$$

where $\mathbf{P}_t = \text{diag}\left(\sigma'\left((\mathbf{A})_{i_t j_t} \mathbf{X}_t^{(j_t)} \mathbf{W}\right)\right)$, and $\mathbf{M}_t = (\mathbf{A})_{i_t j_t} \mathbf{W}^\top$. On the other hand, the Jacobian of the linear recurrent equation (3) of an MP-SSM block, in the static case with a number k of linear recurrent steps computed along the same walk reads:

$$\frac{\partial \mathbf{X}_k^{(i)}}{\partial \mathbf{X}_0^{(j)}} = \prod_{t=0}^{k-1} \mathbf{M}_t.$$

We aim to prove that, for a generic vector \mathbf{x} with entries i.i.d. random variables distributed symmetrically about zero (e.g. according to a Normal distribution with zero mean), it holds the approximation $\|\prod_{t=0}^{k-1} \mathbf{P}_t \mathbf{M}_t \mathbf{x}\| \approx 2^{-\frac{k}{2}} \|\prod_{t=0}^{k-1} \mathbf{M}_t \mathbf{x}\|$. We prove the thesis using a recursive argument. First, we observe that, denoting $\mathbf{y} = \mathbf{M}_0 \mathbf{x}$, then we can write

$$\|\mathbf{P}_0 \mathbf{M}_0 \mathbf{x}\|^2 = \|\mathbf{P}_0 \mathbf{y}\|^2 = (p_1 y_1)^2 + \dots + (p_n y_n)^2. \quad (14)$$

Now, since the p_i are assumed i.i.d. Bernoulli random variables, each with probability $\frac{1}{2}$ of taking the value 0, in the sum of (14), roughly a portion of half of the contributions from \mathbf{y} are zeroed-out due to action of \mathbf{P}_0 . Therefore,

$$\|\mathbf{P}_0 \mathbf{M}_0 \mathbf{x}\|^2 = \|\mathbf{P}_0 \mathbf{y}\|^2 \approx \frac{1}{2} \|\mathbf{y}\|^2 = \frac{1}{2} \|\mathbf{M}_0 \mathbf{x}\|^2. \quad (15)$$

Note that the larger the dimension of the graph n , the more accurate the approximation of (15). Therefore, we conclude that $\|\mathbf{P}_0 \mathbf{M}_0 \mathbf{x}\| \approx 2^{-\frac{1}{2}} \|\mathbf{M}_0 \mathbf{x}\|$. Now, we proceed recursively by denoting $\tilde{\mathbf{x}}_t = \mathbf{P}_{t-1} \mathbf{M}_{t-1} \dots \mathbf{P}_0 \mathbf{M}_0 \mathbf{x}$, and defining the scalars $c_t = \frac{\|\mathbf{M}_t \tilde{\mathbf{x}}_t\|}{\|\tilde{\mathbf{x}}_t\|} > 0$, for all $t = 1, \dots, k-1$. Then, we can write

$$\begin{aligned} \|\mathbf{P}_{k-1} \mathbf{M}_{k-1} \mathbf{P}_{k-2} \mathbf{M}_{k-2} \dots \mathbf{P}_0 \mathbf{M}_0 \mathbf{x}\| &= \\ &= \|\mathbf{P}_{k-1} \mathbf{M}_{k-1} \tilde{\mathbf{x}}_{k-1}\| \approx \\ &\approx 2^{-\frac{1}{2}} \|\mathbf{M}_{k-1} \tilde{\mathbf{x}}_{k-1}\| = \\ &= 2^{-\frac{1}{2}} c_{k-1} \|\tilde{\mathbf{x}}_{k-1}\| = \\ &= 2^{-\frac{1}{2}} c_{k-1} \|\mathbf{P}_{k-2} \mathbf{M}_{k-2} \tilde{\mathbf{x}}_{k-2}\| \approx \\ &\approx 2^{-\frac{1}{2}} c_{k-1} 2^{-\frac{1}{2}} c_{k-2} \|\tilde{\mathbf{x}}_{k-2}\| \approx \dots \\ &\approx 2^{-\frac{k}{2}} c_{k-1} c_{k-2} \dots c_0 \|\mathbf{x}\|. \end{aligned}$$

On the other hand, for the case of MP-SSM, it reads:

$$\begin{aligned} \|\mathbf{M}_{k-1} \mathbf{M}_{k-2} \dots \mathbf{M}_0 \mathbf{x}\| &= c_{k-1} \|\mathbf{M}_{k-2} \dots \mathbf{M}_0 \mathbf{x}\| = \\ &= c_{k-1} c_{k-2} \|\mathbf{M}_{k-3} \dots \mathbf{M}_0 \mathbf{x}\| = \dots \\ &= c_{k-1} c_{k-2} \dots c_0 \|\mathbf{x}\|. \end{aligned}$$

This proves that a standard GCN vanishes information $2^{-\frac{k}{2}}$ faster than MP-SSM.

We assumed weight sharing in the GCN, but the same proof holds assuming different weights $\mathbf{W}_1, \dots, \mathbf{W}_k$ at each GCN layer, by simply using the same exact weight matrices for the linear equation of MP-SSM. \square

B Fast Parallel Implementation

We describe all the details to derive and implement a fast parallel implementation for the computation of an MP-SSM block.

The unfolded recurrence of an MP-SSM block gives the following closed-form solution:

$$\mathbf{X}_{k+1} = \mathbf{A}^k \mathbf{U}_1 \mathbf{B} \mathbf{W}^k + \mathbf{A}^{k-1} \mathbf{U}_2 \mathbf{B} \mathbf{W}^{k-1} + \dots + \mathbf{A} \mathbf{U}_k \mathbf{B} \mathbf{W} + \mathbf{U}_{k+1} \mathbf{B}. \quad (16)$$

Therefore the equation of an MP-SSM block reads:

$$\mathbf{X}_{k+1} = \sum_{i=0}^k \mathbf{A}^i \mathbf{U}_{k+1-i} \mathbf{B} \mathbf{W}^i, \quad (17)$$

$$\mathbf{Y}_{k+1} = \text{MLP}(\mathbf{X}_{k+1}), \quad (18)$$

The closed-form solution of an MP-SSM block tells us that we could implement the whole recurrence in one shot. However, the computation of the powers of both the GSO, \mathbf{A} , and the recurrent weights, \mathbf{W} , can be extremely expensive for generic matrices and large values of k . On the other hand, the powers of diagonal matrices are fairly easy to compute, since they are simply the powers of their diagonal entries. Below, we show how to reduce a generic dense real-valued MP-SSM block to an equivalent diagonalised complex-valued MP-SSM block.

Assume the following diagonalisation of the shift operator: $\mathbf{A} = \mathbf{P} \Lambda \mathbf{P}^{-1}$. If undirected graph, i.e., \mathbf{A} is symmetric, then by spectral theorem the \mathbf{P} is a real orthogonal matrix (i.e. $\mathbf{P}^{-1} = \mathbf{P}^\top$) and Λ is real.

Assume the following diagonalisation of the weights: $\mathbf{W} = \mathbf{V}\Sigma\mathbf{V}^{-1}$. If using dense real matrices as weights, then their diagonalisation is possible only assuming complex matrices of eigenvectors \mathbf{V} and complex eigenvalues Σ . Also, note that the set of defective matrices (i.e. non-diagonalizable in \mathbb{C}) has zero Lebesgue measure [41].

Assume the following MLP equations with 2 layers: $\text{MLP}(\mathbf{X}) = \phi(\mathbf{X}\mathbf{W}_1)\mathbf{W}_2$, where ϕ is a nonlinearity, and $\mathbf{W}_1, \mathbf{W}_2$ real dense matrices.

With the above assumptions, the MP-SSM block equations can be equivalently written as:

$$\mathbf{X}_{k+1} = \sum_{i=0}^k \mathbf{P}\Lambda^i \mathbf{P}^{-1} \mathbf{U}_{k+1-i} \mathbf{B} \mathbf{V} \Sigma^i \mathbf{V}^{-1}, \quad (19)$$

$$\mathbf{Y}_{k+1} = \phi(\mathbf{X}_{k+1} \mathbf{W}_1) \mathbf{W}_2, \quad (20)$$

which we can write as:

$$\mathbf{X}_{k+1} = \mathbf{P} \left(\sum_{i=0}^k \Lambda^i \mathbf{P}^{-1} \mathbf{U}_{k+1-i} \mathbf{B} \mathbf{V} \Sigma^i \right) \mathbf{V}^{-1}, \quad (21)$$

$$\mathbf{Y}_{k+1} = \phi(\mathbf{X}_{k+1} \mathbf{W}_1) \mathbf{W}_2, \quad (22)$$

Multiply on the left side both terms by \mathbf{P}^{-1} and on the right side both terms by \mathbf{V}

$$\mathbf{P}^{-1} \mathbf{X}_{k+1} \mathbf{V} = \sum_{i=0}^k \Lambda^i \mathbf{P}^{-1} \mathbf{U}_{k+1-i} \mathbf{B} \mathbf{V} \Sigma^i \quad (23)$$

If we change coordinate reference to $\mathbf{Z}_{k+1} = \mathbf{P}^{-1} \mathbf{X}_{k+1} \mathbf{V}$, then we can write:

$$\mathbf{Z}_{k+1} = \sum_{i=0}^k \Lambda^i \mathbf{P}^{-1} \mathbf{U}_{k+1-i} \mathbf{B} \mathbf{V} \Sigma^i, \quad (24)$$

$$\mathbf{Y}_{k+1} = \phi(\mathbf{P} \mathbf{Z}_{k+1} \mathbf{V}^{-1} \mathbf{W}_1) \mathbf{W}_2, \quad (25)$$

Equations (24) and (25) give the same exact dynamics of the equations (17) and (18).

The matrix of complex eigenvectors \mathbf{V} in (24) can be merged into the real matrix of weights \mathbf{B} in equation (26). Therefore, we can call $\hat{\mathbf{B}}$ a complex matrix of weights that accounts for the term $\mathbf{B} \mathbf{V}$. Similarly, the matrix eigenvectors \mathbf{V}^{-1} in (25) can be merged into the matrix of weights \mathbf{W}_1 in equation (27), that we call $\hat{\mathbf{W}}_1$. To get an exact equivalence, we should exactly multiply by \mathbf{V} and \mathbf{V}^{-1} , but merging these into learnable complex-valued matrices $\hat{\mathbf{B}}$ and $\hat{\mathbf{W}}_1$ then we get similar performance.

With these new notations, we can write the equivalent diagonalised complex-valued MP-SSM block:

$$\mathbf{Z}_{k+1} = \sum_{i=0}^k \Lambda^i \hat{\mathbf{U}}_{k+1-i} \hat{\mathbf{B}} \Sigma^i, \quad (26)$$

$$\mathbf{Y}_{k+1} = \phi(\mathbf{P} \mathbf{Z}_{k+1} \hat{\mathbf{W}}_1) \mathbf{W}_2, \quad (27)$$

where, in summary:

- input is pre-processed as $\hat{\mathbf{U}}_{k+1-i} = \mathbf{P}^{-1} \mathbf{U}_{k+1-i}$,
- Λ is the diagonal matrix of the eigenvalues of the GSO,
- learnable recurrent weights are $\hat{\mathbf{B}}$ (complex and dense), and Σ (complex and diagonal)
- learnable readout weights are $\hat{\mathbf{W}}_1$ (complex and dense), and \mathbf{W}_2 (real and dense)

Equations (26)-(27) tell us that we can implement the whole recurrence efficiently in a closed-form solution that only involves powers of diagonal matrices.

We provide in Algorithm 1, the pytorch-like implementation of the fast MP-SSM, provided the input sequence $(\hat{\mathbf{U}}_1, \dots, \hat{\mathbf{U}}_{k+1})$, computes in parallel the whole output sequence $(\mathbf{Y}_1, \dots, \mathbf{Y}_{k+1})$.

Algorithm 1 MP-SSM fast implementation

Require: the input features $\mathbf{x} \in \mathbb{C}^{\text{num_steps} \times n \times C}$ (if temporal), else $\mathbf{x} \in \mathbb{C}^{n \times C}$; the number of iterations (i.e., $k+1$) num_steps ; the diagonal complex-valued weight matrix $\mathbf{W} \in \mathbb{C}^{\text{hidden_dim}}$; the complex-valued matrix $\mathbf{B} \in \mathbb{C}^{C \times \text{hidden_dim}}$; the eigenvalues of the GSO $\text{eigenvals} \in \mathbb{C}^n$

Ensure: $\text{out} \in \mathbb{C}^{\text{num_steps} \times n \times \text{hidden_dim}}$

```

1: powers = torch.arange(num_steps)
2:  $\Lambda_{\text{powers}} = \text{eigenvals}.\text{unsqueeze}(-1).\text{pow}(\text{powers})$   $\triangleright$  shape:  $(n, \text{num\_steps})$ 
3:  $\Sigma_{\text{powers}} = \mathbf{W}.\text{unsqueeze}(-1).\text{pow}(\text{powers})$   $\triangleright$  shape:  $(\text{hidden\_dim}, \text{num\_steps})$ 
4: if not temporal then
5:    $\mathbf{x} = \mathbf{x}.\text{repeat}(\text{num\_steps}, 1, 1)$   $\triangleright$  shape:  $(\text{num\_steps}, n, C)$ , static case
6: end if
7:  $\mathbf{x}_{\text{flipped}} = \text{torch}.\text{flip}(\mathbf{x}, \text{dims} = [0])$   $\triangleright$  shape:  $(\text{num\_steps}, n, C)$ 
8:  $\mathbf{x}_{\text{complex}} = \mathbf{x}_{\text{flipped}}.\text{to}(\text{torch}.\text{cfloat})$ 
9:  $\mathbf{x}_B = \text{torch}.\text{matmul}(\mathbf{x}_{\text{complex}}, \mathbf{B})$   $\triangleright$  shape:  $(\text{num\_steps}, n, \text{hidden\_dim})$ 
10:  $\Lambda_{\text{powers}} = \Lambda_{\text{powers}}.\text{permute}(2, 0, 1)$   $\triangleright$  shape:  $(\text{num\_steps}, n, 1)$ 
11:  $\Sigma_{\text{powers}} = \Sigma_{\text{powers}}.\text{transpose}(1, 0).\text{unsqueeze}(1)$   $\triangleright$  shape:  $(\text{num\_steps}, 1, \text{hidden\_dim})$ 
12:  $\text{scaled\_x\_B} = \Lambda_{\text{powers}} \cdot \mathbf{x}_B \cdot \Sigma_{\text{powers}}$ 
13:  $\text{out} = \text{scaled\_x\_B}.\text{cumsum}(\text{dim} = 0)$   $\triangleright$  shape:  $(\text{num\_steps}, n, \text{hidden\_dim})$ 
14:  $d_1, d_2, d_3 = \text{out}.\text{shape}$ 
15:  $\mathbf{x}_{\text{agg}} = \text{out}.\text{permute}(1, 2, 0).\text{reshape}(n, -1)$   $\triangleright$  shape:  $(n, \text{num\_steps} \cdot \text{hidden\_dim})$ 
16:  $\mathbf{x}_{\text{agg}} = \text{matmul}(\mathbf{x} = \mathbf{x}_{\text{agg}},$ 
    $\text{edge\_index} = \text{matrix\_p\_edge\_index},$ 
    $\text{edge\_weight} = \text{matrix\_p\_edge\_weight}$ 
   )
17:  $\mathbf{x}_{\text{agg}} = \mathbf{x}_{\text{agg}}.\text{reshape}(d_2, d_3, d_1).\text{permute}(2, 0, 1)$ 
18:  $\text{out} = \text{mlp}(\mathbf{x}_{\text{agg}}, \text{batch})$ 

```

We acknowledge that there is no free lunch: we achieve a one-shot parallel implementation trading off GPU memory usage, since the whole tensor of shape $(\text{num_steps}, n, \text{hidden_dim})$, in line 9 of Algorithm 1, must fit into the GPU. However, with sufficient GPU memory, the entire MP-SSM block computation occurs in 10^{-3} seconds, see Figure 3. As shown in Figure 3, MP-SSM scales similarly

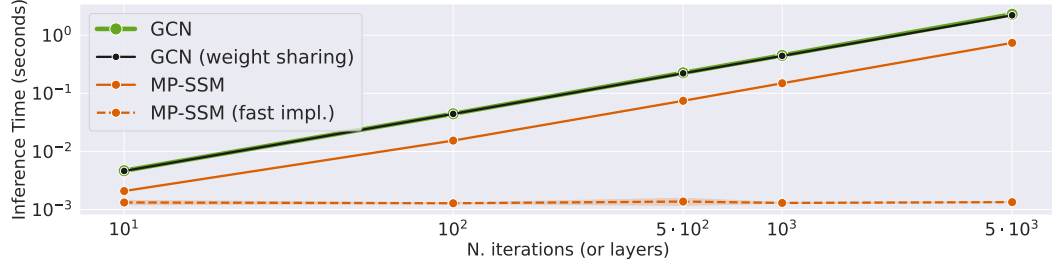


Figure 3: Inference time on a graph of $n = 100$ nodes (with number of edges 3058), input dimension $C = 1$, $\text{hidden_dim} = 32$, and increasing lengths $k = 10, 100, 500, 1000, 5000$. GCN is a standard GCN with tanh without residual with k layers. GCN (weight sharing) is the same, but just one layer iterated k times. MP-SSM baselines use both 1 block.

to GCN and GCN (weight sharing), whose lines are overlapping, but it is slightly faster, owing to the

lack of nonlinearity in the recurrence—a benefit that grows with more iterations. On the other hand, the fast implementation of MP-SSM maintains constant runtime, provided enough GPU memory.

Finally, we note that, unlike standard SSM models such as S4 and Mamba, which follow a Single-Input-Single-Output strategy—computing a separate SSM for each input channel and then mixing the results—our implementation in Algorithm 1 adopts a Multiple-Input-Multiple-Output strategy, enabling native handling of multivariate inputs.

C Relation to other temporal graph models based on state-space modeling

In the recent literature, we can find temporal graph models that leverage the state-space approach. The MP-SSM presents a simplified yet effective recurrent architecture for temporal graph modeling, offering clear advantages in architectural design when compared to alternatives such as GGRNN [90] or GraphSSM [66]. The MP-SSM recurrent dynamics are governed by a simple linear diffusion on the graph:

$$\mathbf{X}_{t+1} = \mathbf{A}\mathbf{X}_t\mathbf{W} + \mathbf{U}_{t+1}\mathbf{B}. \quad (28)$$

In contrast, the GGRNN recurrent equation (in its simplest form, without gating mechanisms) adopts a more elaborate design:

$$\mathbf{X}_{t+1} = \sigma \left(\sum_{j=0}^{K-1} \mathbf{A}^j \mathbf{X}_t \mathbf{W}_j + \sum_{j=0}^{K-1} \mathbf{A}^j \mathbf{U}_{t+1} \mathbf{B}_j \right), \quad (29)$$

where multiple powers of the shift operator, \mathbf{A} , are used to aggregate information from both previous embedding \mathbf{X}_t and current input features \mathbf{U}_{t+1} , weighted with several learnable matrices, \mathbf{W}_j and \mathbf{B}_j , which are applied for different j values, and finally, applying a nonlinearity *at each time step*.

The key distinguishing feature of MP-SSM is the *absence of nonlinearity in the recurrent update*, with the only nonlinear transformation appearing in a downstream MLP decoder, typically composed of two dense layers with an activation function in between. This feature also allows for a fast implementation of the recurrence, since it can be unfolded to get a closed-form solution, see Appendix B. Moreover, in an MP-SSM block, the same weights, \mathbf{W} , \mathbf{B} and MLP parameters, are shared across all time steps, ensuring *strict weight sharing throughout the sequence*. Moreover, our methodology implements a stack of MP-SSM blocks to build richer representations, differently from GGRNN where only one layer of recurrent computation is performed.

On the other hand, the GraphSSM model [66] adopts a strategy of stacking several GraphSSM blocks similar to MP-SSM, but their building blocks are fundamentally different from our MP-SSM block. In fact, a GraphSSM block processes the spatio-temporal input sequence $[\mathbf{U}_t]$ in three main stages, see Appendix D.2 of [66]. First, a GNN backbone is applied to the input sequence, generating a corresponding sequence of node embeddings \mathbf{X}_t . Next, each embedding is mixed with the one from the previous time step \mathbf{X}_{t-1} , producing a smoothed temporal embedding \mathbf{H}_t . This mixed sequence $[\mathbf{H}_t]$ is then treated as a multivariate time series and passed through an SSM layer—such as S4, S5, or S6—to yield the final sequence $[\mathbf{Y}_t]$ as the output of a GraphSSM block. Our approach is conceptually simpler, as it integrates both the GNN diffusive dynamics and sequence-based processing within a unified linear recurrence—Equation (28)—followed by a shared MLP applied across time steps. In this sense, MP-SSM embeds the core principles behind modern SSMs—the very principles that have driven the success of sequential modeling—directly into the graph processing framework. In contrast, GraphSSM merely combines GNN and SSM backbones in a modular fashion to address temporal graph tasks, without deeply integrating their underlying mechanisms.

In Table 5, we provide a direct comparison between MP-SSM, GGRNN, and GraphSSM, on the Metr-LA and PeMS-Bay datasets. To ensure a fair and comprehensive comparison, we computed MAE, RMSE, and MAPE for all three models: MP-SSM, GGRNN, and GraphSSM. We used GGRNN without gating mechanisms, as it achieved the best performance on Metr-LA according to [90, Table IV], and GraphSSM-S4, since the authors reported in [66] that their experiments were primarily conducted using the S4 architecture. As the results show, our method consistently and significantly outperforms both GGRNN and GraphSSM across all three metrics on both datasets.

Table 5: Multivariate time series forecasting on the Metr-LA and PeMS-Bay datasets for Horizon 12. **Best** results for each task are in bold.

Model	Metr-LA			PeMS-Bay		
	MAE ↓	RMSE ↓	MAPE ↓	MAE ↓	RMSE ↓	MAPE ↓
GGRNN	3.88	8.14	10.59%	2.34	5.14	5.21%
GraphSSM-S4	3.74	7.90	10.37%	1.98	4.45	4.77%
MP-SSM (ours)	3.17	6.86	9.21%	1.62	4.22	4.05%

D Multi-hop interpretation of a deep MP-SSM architecture

MP-SSM is fundamentally different from multi-hop GNNs approaches: it operates through strictly 1-hop message passing at each iteration and does not perform aggregation from far-away hops by design. Nonetheless, to better understand its behavior in deeper architectures, we explore how a multi-hop perspective can be used for interpretation, drawing contrasts with a representative multi-hop model, Drew [49]. For this purpose, let us consider the static case, with the input being the sequence $[\mathbf{U}_1, \dots, \mathbf{U}_1]$. The linearity of the recurrent equation of an MP-SSM block allows us to unfold the recurrent equation as follows:

$$\mathbf{X}_{k+1} = \mathbf{A}^{k+1} \mathbf{X}_0 \mathbf{W}^{k+1} + \sum_{i=0}^k \mathbf{A}^i \mathbf{U}_1 \mathbf{B} \mathbf{W}^i. \quad (30)$$

Therefore, assuming a zero initial state and including the MLP into the equation, we have the following expression in the output of the first MP-SSM block:

$$\mathbf{Y}_{k+1} = \text{MLP} \left(\sum_{i=0}^k \mathbf{A}^i \mathbf{U}_1 \mathbf{B} \mathbf{W}^i \right). \quad (31)$$

Due to the various powers of the shift operator $\mathbf{I}, \mathbf{A}, \mathbf{A}^2, \dots, \mathbf{A}^k$, we can interpret Equation (31) as a k -hop aggregation of the input graph \mathbf{U}_1 . Now, the sequence $[\mathbf{Y}_{k+1}, \dots, \mathbf{Y}_{k+1}]$ is the input to the second MP-SSM block. Therefore, stacking the second MP-SSM block, and considering a residual connection from the first MP-SSM block, we have the following expression in the output of the second MP-SSM block:

$$\mathbf{Y}_{2(k+1)} = \mathbf{Y}_{k+1} + \text{MLP} \left(\sum_{i=0}^k \mathbf{A}^i \mathbf{Y}_{k+1} \mathbf{B}_2 \mathbf{W}_2^i \right), \quad (32)$$

where $\mathbf{B}_2, \mathbf{W}_2$, are the shared weights of the second MP-SSM block. In general, in a deep MP-SSM architecture of s blocks, we have the following expression in the output of the s -th MP-SSM block:

$$\mathbf{Y}_{s(k+1)} = \mathbf{Y}_{(s-1)(k+1)} + \text{MLP} \left(\sum_{i=0}^k \mathbf{A}^i \mathbf{Y}_{(s-1)(k+1)} \mathbf{B}_s \mathbf{W}_s^i \right). \quad (33)$$

To reveal the multi-hop view, we denote $\hat{\mathbf{Y}}^{(s)} = \mathbf{Y}_{s(k+1)}$, $\hat{\mathbf{W}}_i^{(s)} = \mathbf{B}_s \mathbf{W}_s^i$, and describe the deep MP-SSM architecture at the granularity of its blocks, as follows:

$$\hat{\mathbf{Y}}^{(s)} = \hat{\mathbf{Y}}^{(s-1)} + \text{MLP} \left(\sum_{i=0}^k \mathbf{A}^i \hat{\mathbf{Y}}^{(s-1)} \hat{\mathbf{W}}_i^{(s)} \right). \quad (34)$$

This multi-hop interpretation of a deep MP-SSM architecture resembles the DRew-GCN architecture [49], a multi-hop MPNN employing a dynamically rewired message passing strategy with delay. In fact, the recurrent equation of DRew-GCN, rephrased in our MP-SSM notation for ease of comparison, is defined as:

$$\mathbf{Y}^{(s+1)} = \mathbf{Y}^{(s)} + \sigma \left(\sum_{i=1}^{s+1} \mathbf{A}(i) \mathbf{Y}^{(s-\tau_\nu(i))} \mathbf{W}_i^{(s)} \right), \quad (35)$$

where $\mathbf{A}(i)$ is the degree-normalised shift operator that considers all the neighbors at an *exact* i hops from each respective root node, $\mathbf{W}_i^{(s)}$ are weight matrices, and $\tau_\nu(i)$ is a positive integer (the *delay*) defining the temporal window for the aggregation of past embeddings. Comparing Equation (34) and Equation (35) we can summarize the following differences:

- DRew aggregates information using $\mathbf{A}(i)$, a function of the GSO that counts neighbors at an *exact* i hops distance, while MP-SSM considers the powers of the GSO, \mathbf{A}^i , thus accounting for all the possible walks of length i . Similarly, the learnable weights in MP-SSM reflect the architectural bias induced by the recurrence, as they are structured through powers of a base matrix, specifically following the form $\hat{\mathbf{W}}_i^{(s)} = \mathbf{B}_s \mathbf{W}_s^i$.
- DRew nonlinearly aggregates information via a pointwise nonlinearity σ , while MP-SSM employs a more expressive 2-layers MLP.
- MP-SSM uses the same features for multi-hop aggregation (corresponding to $\tau_\nu(i) \equiv 0$), whereas DRew aggregates features from previous layers with a delay $\tau_\nu(i) = \max(0, i - \nu)$, effectively introducing a temporal rewiring of the graph.

Although the unfolding of MP-SSM yields expressions involving powers of the GSO, this resemblance to multi-hop architectures such as DRew [49] is purely superficial. Unlike models that aggregate information from distant nodes within a single layer, MP-SSM performs strictly 1-hop message passing at each iteration. The higher-order GSO terms emerge naturally from the recurrence, not from an architectural bias toward multi-hop aggregation. This formulation, grounded in first principles, preserves the original graph topology and constitutes a structurally distinct approach. We provide in Table 6 a comparison of DRew-GCN (results taken from [49]) with our MP-SSM on the Peptides-func and Peptides-struct from the LRGB task [32]. Notably, MP-SSM outperforms DRew-GCN on the Peptides-struct task, suggesting that the structural architectural bias introduced by the recurrence, combined with MLP adaptivity, offers a stronger advantage than aggregating information via rewired connections from delayed past features. In contrast, on the Peptides-func task, the performance of the two models falls within each other’s standard deviation, indicating no statistically significant difference between DRew-GCN—despite its dynamic rewiring strategy with delay—and MP-SSM. In Appendix I we report an extended evaluation on the LRGB benchmark.

Table 6: Results for Peptides-func and Peptides-struct averaged over 3 training seeds. DRew-GCN results are taken from [49]. The **best** scores are in bold.

Model	Peptides-func	Peptides-struct
	AP \uparrow	MAE \downarrow
DRew-GCN	69.96 \pm 0.76	0.2781 \pm 0.0028
MP-SSM (ours)	69.93 \pm 0.52	0.2458 \pm 0.0017

E Ablations

We perform an ablation study to isolate the incremental contribution of each SSM heuristic to the performance gains in reconstructing graph-structural information that depends on learning long-range dependencies; specifically for computing quantities like the diameter of a graph, the single-source-shortest-paths (SSSP), and the eccentricity of a node, see Section 4.1 for more details on these tasks. Results of this ablation are reported in Table 7.

Table 7: Architecture ablation study. Mean test $\log_{10}(MSE)$ and std averaged on 4 random weight initialization on Graph Property Prediction tasks (Section 4.1). The lower, the better. The evaluation include: a nonlinear multilayer GCN (GCN), a linear multilayer GCN (Linear GCN), a linear multilayer GCN with weight sharing (Linear GCN (ws)), Linear GCN (ws) followed by an MLP (1 Block Linear GCN), a stack of multiple 1 Block Linear GCN (Multi-Blocks Linear GCN), and our MP-SSM, which represent a multi-blocks linear GCN with standard deep learning heuristics such as residual connections and normalisation layers between blocks.

Model	Diameter \downarrow	SSSP \downarrow	Eccentricity \downarrow
GCN	0.7424 \pm 0.0466	0.9499 \pm 0.0001	0.8468 \pm 0.0028
Linear GCN	-2.1255 \pm 0.0984	-1.5822 \pm 0.0002	-2.1424 \pm 0.0014
Linear GCN (ws)	-2.2678 \pm 0.1277	-1.5823 \pm 0.0001	-2.1447 \pm 0.001
1 Block Linear GCN	-2.2734 \pm 0.1513	-1.5836 \pm 0.0025	-2.1869 \pm 0.0058
Multi-Blocks Linear GCN	-2.3531 \pm 0.3183	-1.5821 \pm 0.0001	-2.1861 \pm 0.0066
MP-SSM	-3.2353 \pm 0.1735	-4.6321 \pm 0.0779	-2.9724 \pm 0.0271

The ablation conducted reveals that removing the nonlinearity from GCN yields the most significant performance improvement. Introducing weight sharing—effectively incorporating recurrence into the linear graph diffusion process—yields a slight performance boost while considerably reducing the number of parameters. Appending an MLP at the last time step of this linear recurrent architecture does not result in statistically significant gains, except marginally for the Eccentricity task. Likewise, constructing a hierarchical block structure does not noticeably enhance performance. These limited improvements suggest that, for the three tasks considered, the linear recurrence mechanism alone, provided a long enough recurrence, is sufficient to capture meaningful representations to reconstruct graph’s structural information. Finally, incorporating standard deep learning heuristics further strengthens the full MP-SSM architecture, consistently improving performance across all tasks.

F Complexity and Runtimes

We discuss the theoretical complexity of our method, followed by a comparison of runtimes with other methods.

Complexity Analysis. Our MP-SSM consists of a stack of blocks. Each of them performs a linear recurrence of k iterations followed by the application of a nonlinear map, as defined in Equations (3) and (4). Note that k is either the length of the temporal graph sequence or a hyperparameter. Given the similarities between the linear recurrence in MP-SSM and standard MPNNs, described in Section 2, the recurrence retains the complexity of standard MPNNs. Therefore, the Equation (3) is linear in the number of node $|V|$ and edges $|E|$, achieving a time complexity of $\mathcal{O}(k \cdot (|V| + |E|))$, with k the number of iterations. Considering $\mathcal{O}(m)$ the time complexity of the MLP in Equation (4), then the final time complexity of one MP-SSM block is $\mathcal{O}(k \cdot (|V| + |E|) + m)$ in the static case and $\mathcal{O}(k \cdot (|V| + |E| + m))$ in the temporal case.

Runtimes. We provide runtimes for MP-SSM and compare it with other methods, such as Graph GPS and GCN, in Table 8. In all cases, we use a model with 256 hidden dimensions and a varying depth effective by changing the number of recurrences from 2 to 16 in our MP-SSM with 2 MP-SSM blocks, and the number of layers is the depth for other methods. We report the training and inference times in milliseconds, as well as the downstream performance obtained on the Roman-Empire dataset. As can be seen from the results in the Table, our MP-SSM maintains a similar runtime to GCN, which has linear complexity with respect to the graph size, while offering strong performance at the same time. Notably, our MP-SSM achieves better performance than GCN and GPS, and maintains its performance as depth increases, different than GCN. All runtimes are measured on an NVIDIA A6000 GPU with 48GB of memory.

Table 8: Training and Inference Runtime (milliseconds) and obtained node classification accuracy (%) on the Roman-Empire dataset.

Metrics	Method	Depth			
		4	8	16	32
Training (ms)	GCN	18.38	33.09	61.86	120.93
Inference (ms)		9.30	14.64	27.95	53.55
Accuracy (%)		73.60	61.52	56.86	52.42
Training (ms)	GPS	1139.05	2286.96	4545.46	OOM
Inference (ms)		119.10	208.26	427.89	OOM
Accuracy (%)		81.97	81.53	81.88	OOM
Training (ms)	GPS _{GAT+Performer} (RWSE)	1179.08	2304.77	4590.26	OOM
Inference (ms)		120.11	209.98	429.03	OOM
Accuracy (%)		84.89	87.01	86.94	OOM
Training (ms)	MP-SSM	23.19	41.44	72.09	141.82
Inference (ms)		10.93	18.87	38.87	67.59
Accuracy (%)		85.73	88.02	90.82	90.91

G The vanishing gradient tendency in nonlinear MPNNs.

Let us consider a highly connected graph without bottlenecks, such that the transfer of messages from any node to any other node is not affected by issues due to structural properties of the graph. However, in the deep regime, the presence of a nonlinearity at each time step can lead the global sensitivity (as defined in Equation (9)) to be vanishing small.

For an MP-SSM block, the local sensitivity $\mathcal{S}_{ij}(t-s)$ of the features of the i -th node to features of the j -th node after $t-s$ applications of message-passing aggregations, is exactly the norm of the Jacobian of Equation (6), i.e. the norm of the product of the (i, j) -entry of \mathbf{A}^{t-s} and the matrix $(\mathbf{W}^\top)^{t-s}$. For standard MPNN approaches, the local sensitivity has a more complicated expression due to nonlinearities at each aggregation step, but usually there are 3 key contributors: one from several multiplications of the shift operator (akin to \mathbf{A}^{t-s} in our MP-SSM), one from several multiplications of the weights (akin to $(\mathbf{W}^\top)^{t-s}$ in our MP-SSM), and one from several multiplications of the derivative of the nonlinearity evaluated on the sequence of embeddings $\mathbf{D}(s), \mathbf{D}(s+1), \dots, \mathbf{D}(t)$. Usually the nonlinearity is pointwise, so $\mathbf{D}(t)$ is a diagonal matrix with entries usually in $[0, 1]$, thus contributing to vanishing the gradient more and more at each time step. Hence, if the subsequent multiplications of weights and nonlinearity-based terms tend to vanish, while the powers of the shift operator \mathbf{A} are bounded (as it is for the case of the symmetrically normalized adjacency with self-loops, proved in Lemma 4.5) then the local sensitivity tends to vanish for *all pair of nodes*, for $t-s$ large enough. This will be reflected in the global sensitivity, which also will tend to vanish, for $t-s$ large enough. This demonstrates that global sensitivity effectively quantifies the severity of vanishing gradient issues in MPNN models plagued by this problem. Note further that the local sensitivity of the linear recurrence in each block of our MP-SSM has the exact form of $\|(\mathbf{A}^{t-s})_{ij}(\mathbf{W}^\top)^{t-s}\|$, while for standard MPNN approaches with nonlinearities at each time step the vanishing effect will be stronger, as we formally proved for the case of GCN in Theorem 3.13.

H Experimental Details

H.1 Employed baselines

In our experiments, the performance of our method is compared with various state-of-the-art GNN baselines from the literature. Specifically, we consider:

- classical MPNN-based methods, i.e., GCN [61], GraphSAGE [50], GAT [108], Gat-edGCN [13], GIN [117], ARMA [11], GINE [56], GCNII [18], and CoGNN [37];
- heterophily-specific models, i.e., H2GCN [126], CPGNN [125], FAGCN [12], GPR-GNN [19], FSGNN [74], GloGNN [67], GBK-GNN [29], and JacobiConv [112];
- physics-inspired MPNNs, i.e., DGC [113], GRAND [15], GraphCON [91], A-DGN [43], GREAD [20], CDE [122], and TDE-GNN [34];
- Graph Transformers, i.e., Transformer [106, 30], GT [95], SAN [63], GPS [88], GOAT [62], Exphormer [96], NAGphormer [16], GRIT [73], and GraphViT [53];
- Higher-Order DGNs, i.e., DIGL [40], MixHop [1], DRew [49], and GRED [28].
- SSM-based GNN, i.e., Graph-Mamba [110], GMN [10], GPS+Mamba [10], GGRNN [90], and GraphSSM [66].
- Graph-agnostic temporal predictors, i.e., Historical Average (AV), SVR [98], and FC-LSTM [101], and VAR [71];
- Spatio-temporal GNNs, i.e., DCRNN [68], GConvGRU [92], Graph WaveNet [116], AST-GCN [47], STGCN [99], GMAN [124], MTGNN [115], AGCRN [7], T-GCN [123], DyGrae [102], EGCRN-O [83], A3T-GCN [6], MPNN LSTM [82], GTS [93], STEP [94], GC-LSTM [17], DynGESN [76], HMM4G [35], STAEformer [70], RGDAN [36], AdpST-GCN [120], and STD-MAE [39].

H.2 Datasets statistics

In our experiments, we compute the performance of our MP-SSM on widely used benchmarks for both static and temporal graphs. Specifically, we consider:

- long-range propagation tasks, i.e., the three graph property prediction tasks proposed by [43] (“Diameter”, “SSSP”, and “Eccentricity”) and the “Peptide-func” and “Peptide-struct” tasks from the long-range graph benchmark [32];
- heterophilic tasks, i.e., “Roman-empire”, “Amazon-ratings”, “Minesweeper”, “Tolokers”, and “Questions” [86];
- temporal tasks, i.e., “Metr-LA” and “PeMS-Bay” for traffic forecasting [68], and the “Chickenpox Hungary”, “PedalMe London”, and “Wikipedia math” forecasting tasks introduced by [89].

In Table 9, we report the statistics of the employed datasets.

Table 9: Dataset statistics

	Task	Nodes	Edges	Graphs (or Timesteps)	Frequency
Static	Diameter	25 - 35	22 - 553	7,040	—
	SSSP	25 - 35	22 - 553	7,040	—
	Eccentricity	25 - 35	22 - 553	7,040	—
	Peptide-func	150.94 (avg)	307.30 (avg)	15,535	—
	Peptide-struct	150.94 (avg)	307.30 (avg)	15,535	—
	Roman-empire	22,662	32,927	1	—
	Amazon-ratings	24,492	93,050	1	—
	Minesweeper	10,000	39,402	1	—
	Tolokers	11,758	519,000	1	—
	Questions	48,921	153,540	1	—
Temporal	Metr-LA	207	1,515	34,272	5 mins
	PeMS-Bay	325	2,369	52,116	5 mins
	Chickenpox Hungary	20	102	512	Weekly
	PedalMe London	15	225	15	Weekly
	Wikipedia math	731	27,079	1,068	Daily

H.3 Hyperparameter space

In Table 10, we report the grid of hyperparameters employed in our experiments by our method on all the considered benchmarks.

Table 10: The grid of hyperparameters employed during model selection for the graph property prediction tasks (*GPP*), Long Range Graph Benchmark (*LRGB*), heterophilic benchmarks (*Hetero*), and spatio-temporal benchmarks (*Temporal*).

Hyperparameters	Values			
	<i>GPP</i>	<i>LRGB</i>	<i>Hetero</i>	<i>Temporal</i>
Optimizer	Adam	AdamW	AdamW	AdamW
Learning rate	0.003	0.001, 0.0005, 0.0001	0.001, 0.0005, 0.0001	0.005, 0.001, 0.0005, 0.0001
Weight decay	10^{-6}	0, 0.0001, 0.001	0, 0.0001, 0.001	0, 0.0001, 0.001
Dropout	0	0, 0.5	0, 0.4, 0.5, 0.6,	0, 0.5
N. recurrences	1, 5, 10, 20	1, 2, 4, 8, 16	1, 2, 4, 8, 16	1, 2, 4, 8, 16
Embedding dim	10, 20, 30	32,64,128,256	32,64,128,256	32,64,128,256
N. Blocks	1, 2	1, 2, 4, 8, 16	1, 2, 4, 8, 16	1, 2, 4, 8, 16
Structure of \mathbf{U}		$\mathbf{U} = [\mathbf{U}_1, \dots, \mathbf{U}_1]$		$\mathbf{U} = [\mathbf{U}_1, \mathbf{U}_2, \dots]$

I Results on the Long-Range Graph Benchmark.

To further evaluate the performance of our MP-SSM, we consider two tasks of the Long-Range Graph Benchmark (LRGB) [32].

Setup. We evaluate MP-SSM on the Peptides-func and Peptides-struct tasks from the LRGB benchmark, which involve predicting functional and structural properties of peptides that require modeling long-range dependencies. We follow the original experimental setup and 500k parameter budget.

Results. As shown in Table 11, MP-SSM outperforms standard MPNNs, transformer-based GNNs, and most multi-hop and SSM-based models. It achieves the highest average ranking across tasks without relying on global attention or graph rewiring. Compared to other graph SSMs, MP-SSM delivers strong performance while preserving permutation-equivariance.

Table 11: Results for Peptides-func and Peptides-struct averaged over 3 training seeds. Re-evaluated methods employ the 3-layer MLP readout proposed in [104]. Note that all MPNN-based methods include structural and positional encoding. The **first**, **second**, and **third** best scores are colored. Baseline results are reported from [32, 49, 104, 53, 28, 44]. \ddagger means 3-layer MLP readout and residual connections are employed.

Model	Peptides-func AP \uparrow	Peptides-struct MAE \downarrow	avg. Rank \downarrow
MPNNs			
A-DGN	59.75 \pm 0.44	0.2874 \pm 0.0021	26.0
GatedGCN	58.64 \pm 0.77	0.3420 \pm 0.0013	29.0
GCN	59.30 \pm 0.23	0.3496 \pm 0.0013	29.5
GCNII	55.43 \pm 0.78	0.3471 \pm 0.0010	30.5
GINE	54.98 \pm 0.79	0.3547 \pm 0.0045	32.0
GRAND	57.89 \pm 0.62	0.3418 \pm 0.0015	29.0
GraphCON	60.22 \pm 0.68	0.2778 \pm 0.0018	24.0
SWAN	67.51 \pm 0.39	0.2485 \pm 0.0009	12.5
Multi-hop GNNs			
DIGL+MPNN	64.69 \pm 0.19	0.3173 \pm 0.0007	25.0
DIGL+MPNN+LapPE	68.30 \pm 0.26	0.2616 \pm 0.0018	16.5
DRew-GatedGCN	67.33 \pm 0.94	0.2699 \pm 0.0018	19.5
DRew-GatedGCN+LapPE	69.77 \pm 0.26	0.2539 \pm 0.0007	12.0
DRew-GCN	69.96 \pm 0.76	0.2781 \pm 0.0028	14.0
DRew-GCN+LapPE	71.50 \pm 0.44	0.2536 \pm 0.0015	8.0
DRew-GIN	69.40 \pm 0.74	0.2799 \pm 0.0016	17.5
DRew-GIN+LapPE	71.26 \pm 0.45	0.2606 \pm 0.0014	9.5
GRED	70.85 \pm 0.27	0.2503 \pm 0.0019	7.0
MixHop-GCN	65.92 \pm 0.36	0.2921 \pm 0.0023	23.0
MixHop-GCN+LapPE	68.43 \pm 0.49	0.2614 \pm 0.0023	15.5
Transformers			
GraphGPS+LapPE	65.35 \pm 0.41	0.2500 \pm 0.0005	15.5
Graph ViT	69.42 \pm 0.75	0.2449 \pm 0.0016	5.5
GRIT	69.88 \pm 0.82	0.2460 \pm 0.0012	5.0
Transformer+LapPE	63.26 \pm 1.26	0.2529 \pm 0.0016	19.5
SAN+LapPE	63.84 \pm 1.21	0.2683 \pm 0.0043	22.0
Modified and Re-evaluated\ddagger			
DRew-GCN+LapPE	69.45 \pm 0.21	0.2517 \pm 0.0011	11.0
GatedGCN	67.65 \pm 0.47	0.2477 \pm 0.0009	11.0
GCN	68.60 \pm 0.50	0.2460 \pm 0.0007	7.5
GINE	66.21 \pm 0.67	0.2473 \pm 0.0017	12.0
GraphGPS+LapPE	65.34 \pm 0.91	0.2509 \pm 0.0014	17.0
Graph SSMs			
GMN	70.71 \pm 0.83	0.2473 \pm 0.0025	4.5
Graph-Mamba	67.39 \pm 0.87	0.2478 \pm 0.0016	12.5
Ours			
MP-SSM	69.93 \pm 0.52	0.2458 \pm 0.0017	4.0

J Extended comparison on the Heterophilic Benchmark

To further evaluate the performance of MP-SSM, we report a more complete comparison for the heterophilic task in Table 12. Specifically, we include more MPNN-based models, graph transformers, and heterophily-designated GNNs.

In Table 12, we color the top three methods. Different from the main body of the paper, here we also include sub-variants of methods in the highlighted results, providing an additional perspective on the findings. Notably, our MP-SSM achieves the best average ranking across all datasets in the heterophilic benchmarks.

Table 12: Mean test set score and std averaged over 4 random weight initializations on heterophilic datasets. The higher, the better. **First**, **second**, and **third** best results for each task are color-coded. Baseline results are reported from [37, 10, 86, 78, 72]. “*” in the rank column means that the average has been computed over less trials.

Model	Roman-empire Acc \uparrow	Amazon-ratings Acc \uparrow	Minesweeper AUC \uparrow	Tolokers AUC \uparrow	Questions AUC \uparrow	avg. Rank \downarrow
[72]						
MLP-1	64.12 \pm 0.61	38.60 \pm 0.41	50.59 \pm 0.83	71.89 \pm 0.82	70.33 \pm 0.96	41.0
MLP-2	66.04 \pm 0.71	49.55 \pm 0.81	50.92 \pm 1.25	74.58 \pm 0.75	69.97 \pm 1.16	34.4
SGC-1	44.60 \pm 0.52	40.69 \pm 0.42	82.04 \pm 0.77	73.80 \pm 1.35	71.06 \pm 0.92	38.6
Graph-agnostic						
ResNet	65.88 \pm 0.38	45.90 \pm 0.52	50.89 \pm 1.39	72.95 \pm 1.06	70.34 \pm 0.76	37.4
ResNet+adj	52.25 \pm 0.40	51.83 \pm 0.57	50.42 \pm 0.83	78.78 \pm 1.11	75.77 \pm 1.24	32.0
ResNet+SGC	73.90 \pm 0.51	50.66 \pm 0.48	70.88 \pm 0.90	80.70 \pm 0.97	75.81 \pm 0.96	29.0
MPNNs						
CO-GNN(Σ, Σ)	91.57 \pm 0.32	51.28 \pm 0.56	95.09 \pm 1.18	83.36 \pm 0.89	80.02 \pm 0.86	8.0
CO-GNN(μ, μ)	91.37 \pm 0.35	54.17 \pm 0.37	97.31 \pm 0.41	84.45 \pm 1.17	76.54 \pm 0.95	6.8
GAT	80.87 \pm 0.30	49.09 \pm 0.63	92.01 \pm 0.68	83.70 \pm 0.47	77.43 \pm 1.20	18.0
GAT-sep	88.75 \pm 0.41	52.70 \pm 0.62	93.91 \pm 0.35	83.78 \pm 0.43	76.79 \pm 0.71	9.8
GAT (LapPE)	84.80 \pm 0.46	44.90 \pm 0.73	93.50 \pm 0.54	84.99 \pm 0.54	76.55 \pm 0.84	16.0
GAT (RWSE)	86.62 \pm 0.53	48.58 \pm 0.41	92.53 \pm 0.65	85.02 \pm 0.67	77.83 \pm 1.22	11.6
GAT (DEG)	85.51 \pm 0.56	51.65 \pm 0.60	93.04 \pm 0.62	84.22 \pm 0.81	77.10 \pm 1.23	12.6
Gated-GCN	74.46 \pm 0.54	43.00 \pm 0.32	87.54 \pm 1.22	77.31 \pm 1.14	76.61 \pm 1.13	31.4
GCN	73.69 \pm 0.74	48.70 \pm 0.63	89.75 \pm 0.52	83.64 \pm 0.67	76.09 \pm 1.27	25.8
GCN (LapPE)	83.37 \pm 0.55	44.35 \pm 0.36	94.26 \pm 0.49	84.95 \pm 0.78	77.79 \pm 1.34	14.6
GCN (RWSE)	84.84 \pm 0.55	46.40 \pm 0.55	93.84 \pm 0.48	85.11 \pm 0.77	77.81 \pm 1.40	12.0
GCN (DEG)	84.21 \pm 0.47	50.01 \pm 0.69	94.14 \pm 0.50	82.51 \pm 0.83	76.96 \pm 1.21	16.4
SAGE	85.74 \pm 0.67	53.63 \pm 0.39	93.51 \pm 0.57	82.43 \pm 0.44	76.44 \pm 0.62	15.6
Graph Transformers						
Exphormer	89.03 \pm 0.37	53.51 \pm 0.46	90.74 \pm 0.53	83.77 \pm 0.78	73.94 \pm 1.06	16.6
NAQphormer	74.34 \pm 0.77	51.26 \pm 0.72	84.19 \pm 0.66	78.32 \pm 0.95	68.17 \pm 1.53	30.6
GOAT	71.59 \pm 1.25	44.61 \pm 0.50	81.09 \pm 1.02	83.11 \pm 1.04	75.76 \pm 1.66	31.2
GPS	82.00 \pm 0.61	53.10 \pm 0.42	90.63 \pm 0.67	83.71 \pm 0.48	71.73 \pm 1.47	21.4
GPS _{GCN} +Performer (LapPE)	83.96 \pm 0.53	48.20 \pm 0.67	93.85 \pm 0.41	84.72 \pm 0.77	77.85 \pm 1.25	12.8
GPS _{GCN} +Performer (RWSE)	84.72 \pm 0.65	48.08 \pm 0.85	92.88 \pm 0.50	84.81 \pm 0.86	76.45 \pm 1.51	16.6
GPS _{GCN} +Performer (DEG)	83.38 \pm 0.68	48.93 \pm 0.47	93.60 \pm 0.47	80.49 \pm 0.97	74.24 \pm 1.18	22.6
GPS _{GAT} +Performer (LapPE)	85.93 \pm 0.52	48.86 \pm 0.38	92.62 \pm 0.79	84.62 \pm 0.54	76.71 \pm 0.98	14.4
GPS _{GAT} +Performer (RWSE)	87.04 \pm 0.58	49.92 \pm 0.68	91.08 \pm 0.58	84.38 \pm 0.91	77.14 \pm 1.49	15.0
GPS _{GAT} +Performer (DEG)	85.54 \pm 0.58	51.03 \pm 0.60	91.52 \pm 0.46	82.45 \pm 0.89	76.51 \pm 1.19	20.0
GPS _{GCN} +Transformer (LapPE)	OOD	OOD	91.82 \pm 0.41	83.51 \pm 0.93	OOD	33.8
GPS _{GCN} +Transformer (RWSE)	OOD	OOD	91.17 \pm 0.51	83.53 \pm 1.06	OOD	34.4
GPS _{GCN} +Transformer (DEG)	OOD	OOD	91.76 \pm 0.61	80.82 \pm 0.95	OOD	36.2
GPS _{GAT} +Transformer (LapPE)	OOD	OOD	92.29 \pm 0.61	84.70 \pm 0.56	OOD	30.2
GPS _{GAT} +Transformer (RWSE)	OOD	OOD	90.82 \pm 0.56	84.01 \pm 0.96	OOD	33.8
GPS _{GAT} +Transformer (DEG)	OOD	OOD	91.58 \pm 0.56	81.89 \pm 0.85	OOD	36.0
GT	86.51 \pm 0.73	51.17 \pm 0.66	91.85 \pm 0.76	83.23 \pm 0.64	77.95 \pm 0.68	14.4
GT-sep	87.32 \pm 0.39	52.18 \pm 0.80	92.29 \pm 0.47	82.52 \pm 0.92	78.05 \pm 0.93	12.6
Heterophily-Designated GNNs						
CPGNN	63.96 \pm 0.62	39.79 \pm 0.77	52.03 \pm 5.46	73.36 \pm 1.01	65.96 \pm 1.95	40.0
FAGCN	65.22 \pm 0.56	44.12 \pm 0.30	88.17 \pm 0.73	77.75 \pm 1.05	77.24 \pm 1.26	31.0
FSGNN	79.92 \pm 0.56	52.74 \pm 0.83	90.08 \pm 0.70	82.76 \pm 0.61	78.86 \pm 0.92	18.2
GBK-GNN	74.57 \pm 0.47	45.98 \pm 0.71	90.85 \pm 0.58	81.01 \pm 0.67	74.47 \pm 0.86	28.0
GloGNN	59.63 \pm 0.69	36.89 \pm 0.14	51.08 \pm 1.23	73.39 \pm 1.17	65.74 \pm 1.19	41.0
GPR-GNN	64.85 \pm 0.27	44.88 \pm 0.34	86.24 \pm 0.61	72.94 \pm 0.97	55.48 \pm 0.91	38.4
H2GCN	60.11 \pm 0.52	36.47 \pm 0.23	89.71 \pm 0.31	73.35 \pm 1.01	63.59 \pm 1.46	39.6
JacobiConv	71.14 \pm 0.42	43.55 \pm 0.48	89.66 \pm 0.40	68.66 \pm 0.65	73.88 \pm 1.16	36.2
Graph SSMs						
GMN	87.69 \pm 0.50	54.07 \pm 0.31	91.01 \pm 0.23	84.52 \pm 0.21	—	11.0*
GPS + Mamba	83.10 \pm 0.28	45.13 \pm 0.97	89.93 \pm 0.54	83.70 \pm 1.05	—	25.5*
Ours						
MP-SSM	90.91 \pm 0.48	53.65 \pm 0.71	95.33 \pm 0.72	85.26 \pm 0.93	78.18 \pm 1.34	2.4